

AD-A164 978

MECHANICAL FACE SEAL DYNAMICS(U) TECHNION RESEARCH AND  
DEVELOPMENT FOUNDATION LTD HAIFA (ISRAEL)

1/1

I ETSION ET AL. DEC 85 EEC-159 AFMNL-TR-85-2082

UNCLASSIFIED

F49620-83-C-0057

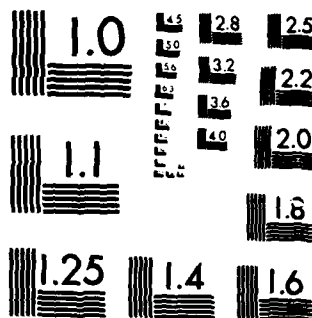
F/G 11/1

NL

END

FILED

15/1



MICROCOPY RESOLUTION TEST CHART  
NATIONAL BUREAU OF STANDARDS-1963-A

AD-A164 978

2

AFWAL-TR-85-2082

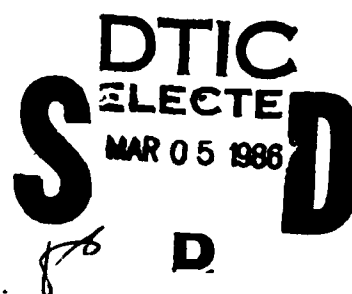
MECHANICAL FACE SEAL DYNAMICS

I. Etsion and I. Green

TECHNION R&D FOUNDATION LTD  
TECHNION, HAIFA 32000, ISRAEL



DECEMBER 1985



FINAL REPORT FOR PERIOD JANUARY 1983 TO AUGUST 1985

APPROVED FOR PUBLIC RELEASE; DISTRIBUTION UNLIMITED

WING FILE COPY

AERO PROPULSION LABORATORY  
AIR FORCE WRIGHT AERONAUTICAL LABORATORIES  
AIR FORCE SYSTEMS COMMAND  
WRIGHT-PATTERSON AIR FORCE BASE, OHIO 45433-6563


86 3 5 0 1 4


## NOTICE

When Government drawings, specifications, or other data are used for any purpose other than in connection with a definitely related Government procurement operation, the United States Government thereby incurs no responsibility nor any obligation whatsoever; and the fact that the Government may have formulated, furnished, or in any way supplied the said drawings, specifications, or other data, is not to be regarded by implication or otherwise as in any manner licensing the holder or any other person or corporation, or conveying any rights or permission to manufacture, use, or sell any patented invention that may in any way be related thereto.


This report has been reviewed by the Office of Public Affairs (ASD/PA) and is releasable to the National Technical Information Service (NTIS). At NTIS, it will be available to the general public, including foreign nations.

This technical report has been reviewed and is approved for publication.

  
GORDON H. GAINER, JR., 1Lt, USAF  
Project Engineer  
Lubrication Branch

  
HOWARD F. JONES  
Chief, Lubrication Branch  
Fuels and Lubrication Division

FOR THE COMMANDER:

  
ROBERT D. SHERRILL, Chief  
Fuels and Lubrication Division  
Aero Propulsion Laboratory

"If your address has changed, if you wish to be removed from our mailing list, or if the addressee is no longer employed by your organization, please notify AFWAL/POSL, WPAFB OH 45433-6563, to help us maintain a current mailing list".

Copies of this report should not be returned unless return is required by security considerations, contractual obligations, or notice on a specific document.

UNCLASSIFIED

SECURITY CLASSIFICATION OF THIS PAGE

ADA 164 978

## REPORT DOCUMENTATION PAGE

1a. REPORT SECURITY CLASSIFICATION UNCLASSIFIED			1b. RESTRICTIVE MARKINGS		
2a. SECURITY CLASSIFICATION AUTHORITY			3. DISTRIBUTION/AVAILABILITY OF REPORT Approved for public release; distribution is unlimited.		
2b. DECLASSIFICATION/DOWNGRADING SCHEDULE					
4. PERFORMING ORGANIZATION REPORT NUMBER(S) EEC-159			5. MONITORING ORGANIZATION REPORT NUMBER(S) AFWL-TR-85-2082		
6a. NAME OF PERFORMING ORGANIZATION Technion R&D Foundation, Ltd.		6b. OFFICE SYMBOL (If applicable) EOARD/LTV		7a. NAME OF MONITORING ORGANIZATION Aero Propulsion Laboratory (AFWL/POSL) Air Force Wright Aeronautical Laboratories	
6c. ADDRESS (City, State and ZIP Code) Technion, Haifa 32000, Israel		7b. ADDRESS (City, State and ZIP Code) Wright-Patterson Air Force Base, Ohio 45433-6563			
8a. NAME OF FUNDING/SPONSORING ORGANIZATION AF Office of Scientific Research		8b. OFFICE SYMBOL (If applicable) EOARD/LTV		9. PROCUREMENT INSTRUMENT IDENTIFICATION NUMBER F49620-83-C-0057	
8c. ADDRESS (City, State and ZIP Code) Box 14, FPO New York 09510		10. SOURCE OF FUNDING NOS.			
		PROGRAM ELEMENT NO. 62203F		PROJECT NO. 3048	TASK NO. 06
				WORK UNIT NO. 29	
11. TITLE (Include Security Classification) MECHANICAL FACE SEAL DYNAMICS					
12. PERSONAL AUTHOR(S) Dr Etsion, Izhak and Dr Green, Itzhak					
13a. TYPE OF REPORT Final		13b. TIME COVERED FROM 1/83 TO 8/85		14. DATE OF REPORT (Yr., Mo., Day) December 1985	
				15. PAGE COUNT 65	
16. SUPPLEMENTARY NOTATION N/A					
17. COSATI CODES			18. SUBJECT TERMS (Continue on reverse if necessary and identify by block number)		
FIELD	GROUP	SUB GR			
21	05		Seals, Mechanical Seals, Noncontacting Seal Dynamics		
19. ABSTRACT (Continue on reverse if necessary and identify by block number)					
<p>This report summarizes a three year study of noncontacting coned-face mechanical seal dynamics. Both small perturbation and full non-linear analyses are presented. An experimental technique to measure relevant dynamic properties of elastomeric secondary seals is described. The critical speed, for the dynamic stability threshold, and the critical rotor runout are presented. It is shown that the more simple to use small perturbation analysis gives very good results for most practical cases.</p> <p><i>This document includes information on the following four areas:</i></p>					
20. DISTRIBUTION/AVAILABILITY OF ABSTRACT UNCLASSIFIED/UNLIMITED <input checked="" type="checkbox"/> SAME AS RPT. <input type="checkbox"/> DTIC USERS <input type="checkbox"/>			21. ABSTRACT SECURITY CLASSIFICATION UNCLASSIFIED		
22a. NAME OF RESPONSIBLE INDIVIDUAL Lt Gordon H. Gainer, Jr.			22b. TELEPHONE NUMBER (Include Area Code) (513) 255-7230		22c. OFFICE SYMBOL AFWL/POSL

DD FORM 1473, 83 APR

EDITION OF 1 JAN 73 IS OBSOLETE.

UNCLASSIFIED

SECURITY CLASSIFICATION OF THIS PAGE

## PREFACE

This final report describes the work performed by Technion Research and Development Foundation Ltd., Technion, Haifa 32000, Israel, under U.S. Air Force Contract F49620-83-C-0057. The report covers the period from January 1983 through August 1985.

This study of noncontacting coned-face mechanical seal dynamics was sponsored by the Aero Propulsion Laboratory of the Air Force Wright Aeronautical Laboratories (AFWAL), Wright-Patterson Air Force Base, Ohio 45433-6563 under project 3048, "Fuels, Lubrication and Fire Protection", Task 304806, "Aerospace Lubrication", Work Unit 30480629, "Mechanical Face Seal Dynamics". Lt G. Gainer and R. Dayton were the USAF AFWAL/POSL Project Engineers. The work at Technion was performed by Dr I. Etsion, who was the Principal Investigator, and Dr I. Green.

Accession For	
NTIS	CRA&I
DTIC	TAB
Unannounced	<input checked="checked" type="checkbox"/>
Justification	<input type="checkbox"/>
By	
Distribution /	
Availability Codes	
Dist	Avail and/or Special



## CONTENTS

I	INTRODUCTION	1
II	APPROACH	3
III	MAIN RESULTS AND CONCLUSIONS	4
	REFERENCES	6
	APPENDIX A	
	1) Stiffness and Damping Characteristics of Elastomer O-Rings Secondary Seals Subjected to Reciprocating Twist,	A-1
	APPENDIX B	
	2) A Kinematic Model for Mechanical Seals with Antirotation Locks or Positive Drive Devices,	B-1
	APPENDIX C	
	3) Stability Threshold and Steady-State Response of Noncontacting Coned-Face Seals, and	C-1
	APPENDIX D	
	4) Nonlinear Dynamic Analysis of Noncontacting Coned-Face Mechanical Seals ,	D-1

## SECTION I

### INTRODUCTION

Radial face seals are used in a host of applications to seal liquids of various types. These liquids range from lubricants to highly toxic chemicals and acids. The applications range from helicopter transmissions to nuclear reactor cooling pumps and submarine propeller shafts. The function of these seals is to restrict the leakage of the sealed fluid and to prevent the entry of solid and liquid debris. A seal permits a rotating shaft to penetrate an enclosure (transmission box, submarine hull, pump housing, etc.) while maintaining separation of the environments on the inside and outside of the enclosure. To do this, one component of the seal is attached to the shaft and rotates with it, and the other component is attached to the housing and is non-rotating. One of the two components is flexibly mounted to provide angular and axial freedom of motion. Mechanical forces and fluid film pressures should tend to force the flexibly mounted face into alignment with the other component. Relative sliding motion takes place between the faces of these two components. In order to avoid wear and to achieve long life, these two sealing faces must be separated by a film of the sealed liquid. This film must be very thin to keep the leakage rate within acceptable limits. Thus, the requirements of lubrication and leakage tend to be conflicting.

There have been many hypotheses put forth to explain the mechanisms responsible for the development of the lubricating film pressure that acts to separate the primary seal faces. These hypotheses include the following: surface angular misalignment, surface waviness, surface asperities, vaporization of the fluid film, axial vibration, and thermal deformation. A good



review of the state-of-the-art is given in Reference 1, and some of the latest results on seal theory are presented in References 2-8. Examination reveals that these published theories are of very limited use from an operation prediction standpoint. Briefly stated, face seal lubrication theory is very primitive as compared to journal bearing theory. Classical journal bearing theory applies to face seal lubrication, but seal dynamics, which is thought to be of major importance, is poorly understood.

Dynamic instability in the form of vibration of flexibly mounted elements was experimentally observed in face type seals (References 9-13). However, only a few attempts have been made so far to analyze seal dynamics. Most of these analyses overlook some of the fluid film or flexible support effects (References 14-18). A fuller treatment of the problem is presented in Reference 19, but it treats a special case and does not offer general design criteria. In more recent work (References 20-22) the motion of a flexibly mounted ring of a noncontacting face seal is described in its three major degrees of freedom (one axial and two angular). Hydrodynamic, hydrostatic, and squeeze film effects, as well as the contribution of the springs of the flexible support, are considered and it is shown how the seal stability is affected by various design parameters. The analysis in References 20-22 is, however, somewhat limited in that it does not contain the effect of an elastomeric secondary seal which often exists in face seals. This element adds both stiffness and damping to the flexible support but the stiffness and damping coefficients are not constants. In the case of seal-rotor runout, the stiffness and damping coefficients of the elastomer are frequency dependent which complicates the solution of the dynamic problem.

The general thrust of this work is aimed at studying the dynamic properties of elastomeric secondary seals and incorporating their effects in a dynamic analysis of mechanical face seals.

## SECTION II

### APPROACH

The effort was divided into three main tasks. Task 1 was devoted to studying experimentally the dynamic properties of elastomeric O-rings. A test rig to simulate the behavior of secondary seal O-rings in a practical mechanical seal was built. Stiffness and damping coefficients of O-rings of various sizes and materials were measured for a range of frequencies and amplitudes. This effort is described in Appendix A.

Task 2 was devoted to developing the kinematic model of a mechanical seal and studying the effect of anti-rotation locks (Appendix B). Following this study the dynamic behavior of a non-contacting, coned-face mechanical seal was analyzed. The analysis was based on linearization of the equations of motion of the flexibly mounted element of the seal. This approach yielded analytical expressions and enabled parametric investigation of the stability threshold and steady state response of the seal (see Appendix C).

During the third task, the complete non-linear dynamic analysis of the seal was performed. A numerical code was developed to solve the non-linear equations of motion of the flexibly mounted element. A comparison was made between the results obtained from the non-linear analysis and those obtained analytically from the small perturbation analysis of Task 2. This effort is described in Appendix D.

### SECTION III

#### MAIN RESULTS AND CONCLUSIONS

1. In practical seals, the dynamic properties of the secondary seals' O-rings are negligibly affected by seal runout. Increasing the shaft speed results in higher stiffness coefficient of elastomer O-rings but may either increase or decrease the damping coefficient depending on the elastomer material. The stiffness  $K$  and damping  $D$  can be expressed by an exponential function

$$K = A\omega^B$$

$$D = a\omega^b$$

where  $\omega$  is the shaft speed and  $A$ ,  $B$ ,  $a$ , and  $b$  are constants related to elastomer material and geometry. Stiffness provided by the secondary seal O-rings is generally much higher than that of mechanical springs.

2. A stability threshold can be found in terms of a critical shaft speed below which stable seal operation is assured. This critical speed is normally very high and, hence, stability threshold should not be a problem in most practical applications. It may become a problem in cases where the shaft speed is very high, stator has a large mass and sealed pressure is low.
3. Non-contacting seals operate with relative misalignment between the mating faces. This relative misalignment depends, among other parameters, on the runout of the rotor and is usually a function of time too, varying cyclically at the shaft frequency.

4. A critical rotor runout exists which, if exceeded, may cause failure by local rubbing contact between the mating faces of the seal due to a too high relative misalignment.
5. Failure because of an excessive leakage resulting from an increase in seal clearance due to rotor runout is likely to occur much before the critical runout is reached. This can happen in seals with low stiffness of the fluid film and flexible support. Small design clearance, high sealed pressure and optimum coning provide high stiffness of the fluid film and reduce the danger of a too high operating clearance.
6. A comparison of the results obtained from a small perturbation analysis and a full non-linear analysis shows a very good correlation for most cases of practical applications. Fair correlation exists even in cases which are clearly out of the range of small perturbation. In these cases, the more simple small perturbation analysis yields results that are on the safe side with regard to the critical rotor runout. Hence, the analytical results of the small perturbation analysis can be used safely over the full range of design parameters and operation conditions.

## REFERENCES

1. Ludwig, L.P. and Greiner, H.F.: Designing Mechanical Face Seals for Improved Performance , Part 2 - Lubrication. Mech. Engrg., Vol. 100, No. 12, Dec. 1978, pp. 18-23.
2. Nau, B.S.: Observation and Analysis of Mechanical Seal Film Characteristics. Jour. of Lub. Tech., Trans. ASME, Vol. 102, No. 3, July 1980, pp. 341-349.
3. Lebeck, A.O.: A Mixed Friction Hydrostatic Face Seal Model with Phase Change, Jour. of Lub Tech., Trans. ASME, Vol. 102, No. 2, April 1980, pp. 133-138.
4. Hughes, W.F. and Cho, N.H.: Phase Change in Liquid Face Seals. II - Isothermal and Adiabatic Bounds with Real Fluids. Jour. of Lub. Tech., Trans. ASME, Vol. 102, No. 3, July 1980, pp. 350-367.
5. Etsion, I. and Sharoni, A.: Performance of End Face Seals with Diametral Tilt and Coning - Hydrostatic Effects. ASLE Trans., Vol. 23, No. 3, July 1980, pp. 279-288.
6. Sharoni, A. and Etsion, I.: Performance of End Face Seals with Diametral Tilt and Coning - Hydrodynamic Effects, ASLE Trans., Vol. 24, No. 1, Jan. 1981, pp. 61-70.
7. Etsion, I.: Squeeze Effects in Radial Face Seals, Jour. of Lub. Tech., Trans. ASME, Vol. 102, No. 2, April 1980, pp. 145-152.

8. Banerjee, B.N. and Burton, R.A.: Experimental Studies on Thermoelastic Effects in Hydrodynamically Lubricated Face Seals. Jour. of Lub. Tech., Trans. ASME, Vol. 101, No. 3, July 1979, pp. 275-282.
9. Matt, R.J.: High Temperature Metal Bellows Seals for Aircraft and Missile Accessories. J. Engng. for Industry. Trans. ASME, Vol 85, Aug. 1963, pp. 281-288.
10. Hudelson, J.C.: Dynamic Instability of Undamped Bellows Face Seals in Cryogenic Liquid. ASLE Trans., Vol. 9, No. 4, Oct. 1966, pp. 381-390.
11. Storm, T.N. Ludwig, L.P. and Hudelson, J.C.: Vibration of Shaft Face Seals and Stabilizing Effect of Viscous and Friction Damping. NASA TN D-5161, April 1969.
12. Kaneta, M., Fukahori, M. and Hirano, F.: Dynamic Characteristics of Face Seal, Proc. 8th Int. Conf. on Fluid Sealing, BHRA, Sept. 1978, paper A2.
13. Etsion, I. and Burton, R.A.: Observation of Self Excited Wobble in Face Seals. Jour. of Lub. Tech., Trans. ASME, Vol. 101, No. 4, Oct. 1979, pp. 526-528.
14. Haardt, R. and Godet, M.: Axial Vibration of a Misaligned Radial Face Seal Under a Constant Closure Force. ASLE Trans., Vol. 18, No. 1, Jan. 1975, pp. 56-61.
15. Zorowski, C.F. and Hill, H.H.: Post Mechanical Separation in Elastically Supported Rotary Face Seals. ASLE Trans., Vol. 14, No. 1, Jan. 1971, pp.75-80.

16. Chaing, T. and Cheng, H.S.: An Analysis of Flexible Seal Ring Vibrations. ASLE Trans., Vol. 11, No. 3, July 1968, pp. 204-215.
17. Griskin, E.N.: The Effect of Dynamics on Fluid Flow in a Face Seal. Proc. 7th Int. Conf. on Fluid Sealing, BHRA, Sept. 1975, paper B2.
18. Kupperman, D.S., Dynamic Tracking of Noncontacting Face Seals. ASLE Trans., Vol. 18, No. 4, Oct. 1975, pp. 306-311.
19. Shapiro, W. and Colsher, R.: Steady State and Dynamic Analysis of a Jet Engine, Gas-Lubricated Shaft Seal. ASLE Trans., 17, No. 3, July 1974, pp. 190-200.
20. Etsion, I. and Dan, Y.: An Analysis of Mechanical Face Seal Vibrations. Jour. of Lub. Tech. Trans. ASME, Vol. 103, No.3, July 1981, pp. 428-435.
21. Etsion, I.: Dynamic Response to Rotating-Seal Runout in Non-Contacting Face-Seals. Jour. of Lub. Tech. Trans. ASME, Vol. 103, No.4. Oct. 1981, pp. 587-592.
22. Etsion, I.: The Accuracy of the Narrow Seal Approximation in Analyzing Radial Face Seals. ASLE Trans., Vol. 23, No. 2, April 1980, pp. 208-216.

APPENDIX A  
STIFFNESS AND DAMPING CHARACTERISTICS OF  
ELASTOMER O-RINGS SECONDARY SEALS SUBJECTED  
TO RECIPROCATING TWIST



# FLUID SEALING

Innsbruck, Austria: 3-5 April, 1984

## STIFFNESS AND DAMPING CHARACTERISTICS OF ELASTOMER O-RINGS SECONDARY SEALS SUBJECTED TO RECIPROCATING TWIST

I. Green and I. Etsion

Department of Mechanical Engineering  
Technion, Israel Institute of Technology  
Haifa, Israel

### Summary

A test is described which simulates forced vibration conditions of an O-ring secondary seal in a mechanical face seal. The O-ring cross section is subjected to a reciprocating harmonic twist similar to that resulting from a rotor runout in an actual seal. Stiffness and damping coefficients of various elastomer O-rings were measured and are presented for a range of forcing amplitudes at frequencies from 100 to 300 Hz. The effects of elastomer material, O-ring geometry, and vibration amplitude and frequency are discussed.

Held at the Innsbruck Congress Centre  
Organised and sponsored by  
BHRA The Fluid Engineering Centre, Cranfield,  
Bedford, MK43 0AJ, England  
©BHRA The Fluid Engineering Centre, 1984

# NOMENCLATURE

$A, a$	} = constants
$B, b$	
$D$	= damping coefficient, Ns/m
$F$	= force, N
$K$	= stiffness coefficient, N/m
$K^*$	= complex stiffness of elastomer
$m$	= mass, kg
$t$	= time, sec
$x$	= mass displacement relative to base, m
$x_0$	= mass amplitude relative to base, m
$y$	= base displacement, m
$y_0$	= base amplitude, m
$\alpha$	= transmissibility, $x_0/y_0$
$\eta$	= loss coefficient, $D\omega/K$
$\phi$	= phase shift, rad
$\omega$	= frequency, rad/s

## 1. INTRODUCTION

A mechanical face seal (Fig. 1) is a complex dynamic system. The rotating seat with its unavoidable axial runout forces both axial and angular vibrations of the flexibly mounted ring. This can be schematically described by the simplified single degree of freedom model in Fig. 2. The harmonic motion of the seat is transmitted via the fluid film to the flexibly mounted ring represented by the mass  $m$ . The flexible support of the seal ring consists of springs in conjunction with a secondary seal element. In many cases this secondary seal is an elastomer O-ring having stiffness  $K_e$  and damping  $D_e$  which affect the dynamic behavior of the entire seal system. In Ref. (1) an order of magnitude of the stiffness and damping coefficients of various components of the seal system is assessed. The O-ring stiffness is shown to be about two orders of magnitude less than the fluid film stiffness but about an order of magnitude higher than the springs stiffness. The O-ring damping is estimated about four orders of magnitude less than the fluid film damping, but this is the only damping provided by the flexible support.

In spite of its relative importance, the effect of the elastomer O-ring on face seal dynamics was not considered in seal analyses published so far. A step in the right direction was made in Ref. (2). Axial forces transmitted by O-rings subjected to a reciprocating drag were measured for various amplitudes and frequencies. However, for a general dynamic analysis the stiffness and damping coefficients of the O-ring, not the forces, are required.

An excellent source on dynamic properties of elastomers is provided in Ref. (3). A main conclusion emerging from this source is that no solid theoretical prediction of elastomers dynamic characteristics is available at present. Stiffness and damping coefficients can at best be measured and are found to be affected by composition, geometry, frequency, strain, temperature, and preload.

While a great deal of information has been gathered on various elastomer springs and dampers this is not the case for O-rings. Refs. (4) and (5) present results on measured dynamic properties of elastomer O-rings under reciprocating radial squeeze, similar to the mode of application in squeeze film dampers. The secondary seal O-ring in a mechanical face seal is, however, subjected to a reciprocating twist of its cross section. This mode of operation is the result of the flexibly mounted ring tracking the axial runout of the rotating seat. No information on the dynamic characteristics of O-rings under reciprocating harmonic twist of their cross section is available in the literature. This report describes an effort to obtain such missing information which is vital for better understanding of mechanical seals dynamics.

## 2. BACKGROUND

Elastomers are characterized by stress relaxation whereby the load required to maintain a constant strain decreases with time. If a load cycle is applied repeatedly to an elastomer element, the process of relaxation causes hysteresis which in turn results in loss of energy per each cycle. Hence, elastomers under cyclic loading provide energy dissipation or hysteretic damping.

The force and displacement in a linear elastomer element undergoing a repeated deflection cycle  $x = x^* e^{i\omega t}$  may be related by (Ref. 3).

$$F = k^* x \quad (1)$$

where  $k^*$  is a complex number in the form

$$k^* = k_1 + ik_2, \quad (2)$$

and is generally a function of frequency, temperature, dynamic strain and geometry, as well as material composition. The quantities  $k_1$  and  $k_2$  are generally referred to as the stiffness and damping of the elastomer. The damping ability of an elastomer element is sometimes expressed in terms of a loss coefficient  $\eta$  which is a nondimensional ratio of the energy dissipated per cycle to the energy stored at maximum displacement

$$\eta = \frac{k_2}{k_1} \quad (3)$$

Various test methods for determining the dynamic properties of elastomers are described in Ref. (3). Of all these methods the most advanced one is the Base Excitation Resonant Mass (BERM) test method, which is described schematically in Fig. 3. By measuring independently the motion of the base  $y = y(t)$ , the motion of mass  $x = x(t)$  relative to the base, and the phase shift  $\phi$  between these two motions, the stiffness and damping of the elastomer can be found. Assuming the Kelvin-Voigt model for the elastomer as shown in Fig. 3, we have

$$m(\ddot{x} + \ddot{y}) + D\dot{x} + Kx = 0 \quad (4)$$

where  $D$  and  $K$  are the damping and stiffness coefficients, respectively, of the elastomer. Assuming a base excitation of the form

$$y = y_0 \sin(\omega t + \phi) \quad (5)$$

and a mass response relative to the base

$$x = x_0 \sin \omega t \quad (6)$$

eq. (4) becomes

$$-m\omega^2 x_0 \sin \omega t + D\omega x_0 \cos \omega t + Kx_0 \sin \omega t = m\omega^2 y_0 \sin(\omega t + \phi) \quad (7)$$

Equating terms containing  $\sin \omega t$  and  $\cos \omega t$  separately we find

$$D = m\omega \frac{\sin \phi}{\alpha} \quad (8)$$

$$K = m\omega^2 \left( \frac{\cos \phi}{\alpha} + 1 \right) \quad (9)$$

where  $\alpha$  is the ratio of the relative response amplitude  $x_0$  to the base excitation amplitude  $y_0$ ,  $\phi$  is the phase shift between  $x$  and  $y$  and  $\omega$  is the frequency of excitation.

The stiffness and damping coefficients  $K$  and  $D$  are related to  $k_1$  and  $k_2$  of eq. (2) in the form

$$k_1 = K \quad (10a)$$

$$k_2 = D\omega \quad (10b)$$

Hence, by eqs. (8) to (10), the loss coefficient  $\eta$  of eq. (3) is

$$\eta = \frac{\sin \phi}{\alpha + \cos \phi} \quad (11)$$

### 3. EXPERIMENTAL SETUP AND TEST PROCEDURE

A test rig was set up as shown in Fig. 4 to obtain the stiffness and damping coefficients of various elastomer O-rings subjected to reciprocating twist of their cross section. A holder (1) attached to the vibrating table (2) of an electromagnetic shaker is holding the base (3) by means of the screw (4). Three different base sizes were used to accommodate an O-ring (5) of 76.2 mm mean outer diameter with three different nominal cross section diameters of 1.78 mm, 3.53 mm, and 5.33 mm (1/16", 1/8", and 3/16"). A mass of 1 kg in the form of an annular ring (6) was fitted on the O-ring. The size of the O-ring groove, and the inner diameter of the ring were selected from ref. (6) for industrial O-ring static seals. This provided a 31 percent squeeze for the 1/16" O-ring and 20 percent squeeze for both the 1/8" and 3/16" O-rings. Two M60 Dymac eddy current proximity probes (7) and (7a) were used to measure the base motion  $y=y(t)$  and the mass motion relative to the base  $x = x(t)$ , respectively.

A data acquisition system based on a PDP 11/40 minicomputer was used to record the probes output and to analyze the data. The two signals  $y(t)$  and  $x(t)$  were

sampled at a rate of 1000 Hz after proper filtration and amplification. Tests were conducted at three different amplitudes,  $y_0$ , of the vibrating base. The amplitudes were 13  $\mu\text{m}$ , 16  $\mu\text{m}$ , and 20  $\mu\text{m}$ . These amplitudes are small enough to prevent slippage of the mass ring on the O-ring but are of the same order of seal seat motion due to seat runout in practical face seals. It was important to prevent slippage of the mass ring in order to eliminate the effect of coulomb friction on the dynamic properties of the O-rings.

Ten different frequencies in the range 100 Hz to 300 Hz were selected for the tests. At each one of the preselected frequencies the shaker amplitude  $y_0$  was maintained constant. The output of the probe monitoring the base motion was observed on a digital voltmeter to facilitate control of the shaker amplitude. Output of the two proximity probes was also observed on an oscilloscope to detect any possible unusual behavior of the test rig (like mass slippage, for example). Only test points which looked satisfactory were recorded and stored in the computer. This procedure was repeated for each of the three different amplitudes  $y_0$ . Several tests were rerun after taking the O-ring off the rig and reassembling again in order to check the repeatability of the results. All tests were run at room temperature which was about 25° C.

A spectral analysis code was used to find the discrete frequency  $\omega$  at each test point along with the corresponding transmissibility  $\alpha$ , and phase shift  $\phi$ . Equations (8), (9) and (11) were then used to calculate the stiffness, damping, and loss coefficients, respectively. As a final step a least square procedure was utilized to find a best fit for the collection of data points. This provided expressions for the stiffness and damping as functions of the frequency, at a constant amplitude  $y_0$ , in the exponential form

$$K = A\omega^B \quad (12)$$

and

$$D = a\omega^b \quad (13)$$

where A, B, a, and b are constants related to the elastomer material and to the O-ring geometry. The expression for the loss coefficient, according to eq. (11) and eqs. (12), (13), is simply

$$\eta = \frac{a}{A} \omega^{(b-B+1)}$$

#### 4. RESULTS AND DISCUSSION

Results of the stiffness, damping and loss coefficients of Nitrile (Buna N) and Fluorocarbon (Viton 75) elastomer O-rings are presented in Figs. 5, 6 and 7 respectively. Varying the amplitude  $y_0$  in the investigated range which was  $13\mu\text{m} \leq y_0 \leq 20\mu\text{m}$  changed the dynamic properties by less than 2%. Hence, no distinction is made in Figs. 5 to 7 between the various amplitudes. Scatter of the test results after reassembling the test rig, as described in the previous section, was up to 30% as can be seen from Figs. 5a and 6a in the case of the Buna N with 1/8" cross section diameter. It should be noticed, however, that for each given O-ring assembly the behaviour was consistent and the data points were lined quite accurately along a straight line on the log - log scale, obeying the relations (12) and (13). Apparently the stiffness and damping are sensitive to some factor related to the mode of assembling O-ring in the test rig (which could be initial twist, for example).

The effect of O-ring cross section diameter is the same in both materials. The smallest diameter provides the highest stiffness and damping. This is partly attributed to the higher squeeze which was 31 percent for the 1/16" diameter O-ring compared to 20 percent for the 1/8" and 3/16" diameters. However, most of the difference in stiffness and damping is due to the change in diameter as can be seen from the results of the two larger diameter O-rings.

The effect of elastomer material is very distinct. In general the Viton 75 has stiffness that is about twice the stiffness of Buna N for the same frequency (Fig. 5). The damping of Viton 75 is about five times larger than that of Buna N in the frequency range of the tests (Fig. 6).

Increasing the frequency increases the stiffness in both Viton 75 and Buna N (Fig. 5). The damping coefficient, however, behaves differently for the two materials

and while an increase in frequency increases the damping of Buna N (Fig. 6a) it reduces the damping of Viton 75 (Fig. 6b). A reduction in damping coefficient with increasing frequency was also observed in Refs. (4) and (5) for various elastomer materials when O-rings were subjected to radial squeeze oscillation. The loss coefficient of the two materials increases with the frequency (Fig. 7).

Table 1 summarizes the results in terms of the constants A, B, a, and b of equations (12) and (13). In general, for the range of frequencies tested, the stiffness coefficient of Viton 75 was between 0.7 MN/m to 4 MN/m and its damping between 0.8 to 5 kN s/m. The stiffness coefficient of the Buna N was between 0.4 to 2 MN/m and its damping coefficient between 0.25 to 0.8 kN s/m. These values are of the same order of magnitude that was assessed in Ref. (1). The stiffness and damping coefficients reported here are also of the same order of magnitude of these reported in Ref. (4) for Viton 70 and Buna N O-rings of similar geometry under reciprocating radial squeeze.

## 5. CONCLUDING REMARKS

A test program for measuring stiffness and damping coefficients of elastomer O-rings is described. The O-rings are subjected to a reciprocating twist of their cross section, similar to the mode of operation of secondary seals in mechanical face seals. Effects of elastomer material, geometry, frequency and amplitude of vibration were examined. It was found that in the range of tested frequencies and base amplitudes (100 to 300 Hz, and 13 to 20  $\mu$ m) the amplitude effect on the dynamic characteristics is negligible. In practice the amplitude depends on the amount of runout. Hence, it may be concluded that in practical seals the dynamic properties of the secondary seals O-rings are independent of the amount of seal runout.

Increasing the frequency of vibration results in a higher stiffness coefficient of elastomer O-rings but may either increase or decrease the damping coefficient depending on the elastomer material. Larger cross section diameters provide lower stiffness and damping.

Both stiffness and damping coefficients can be expressed by an exponential function

$$\begin{aligned} K &= A\omega^B \\ \text{and} \\ D &= a\omega^b \end{aligned}$$

where A, B, a and b are constants related to elastomer material and geometry. In general the stiffness provided by a secondary seal O-ring may be much higher than that of the mechanical springs found in the flexible support of mechanical seals. The damping provided by the O-ring is the only damping in the support. Hence, dynamic properties of secondary seals O-rings have to be thoroughly considered in seal analysis and design.

## 6. ACKNOWLEDGEMENT

The research reported here was supported in parts by the Israel Academy of Sciences and the U.S. Air-Force under contract F 49620-B3-C-0057.

## 7. REFERENCES

1. Rowles, R.T. and Nau, B.S., "An Assessment of Factors Affecting the Response of Mechanical Face Seals to Shaft Vibration, Proc. 18th Inter. Conf. on Fluid Sealing, BHRA, 1978, paper A3.
2. Kittmer, C.A. and Metcalfe, R., "An Inside View of Rotary Seal Dynamics", Proc. of the 5th Symp. on Eng. Applications of Mechanics, Univ. of Ottawa, June, 1980.
3. Darlow, M. and Zorzi, E., "Mechanical Design Handbook of Elastomers", NASA Contractor Report 3423, June 1981.
4. Smalley, A.J., Darlow, M.S. and Mehta, R.K., "The Dynamic Characteristics of O-rings" ASME Trans., Jour. of Mechanical Design, Vol. 100, No. 1, Jan. 1978, pp. 132-138.
5. Kazimierski, Z., and Jarzecki, K., "Stability Threshold of Flexibly Supported Hybrid Gas Journal Bearings", ASME Trans., Jour. of Lub. Tech., Vol. 101, No. 4, Octo. 1979, pp. 451-457.
6. O-ring Handbook, Parker Hannifin Corp., O-ring Division.

Material	cross section diameter	stiffness $K=A\omega^B$		Damping $D=a\omega^b$	
		A	B	a	b
Buna N	1/16"	$3.62 \times 10^5$	0.209	12.45	0.536
	1/8 "	$4.87 \times 10^4$	0.342	15.45	0.483
	3/16"	$1.27 \times 10^5$	0.187	2.76	0.680
Viton 75	1/16"	$1.78 \times 10^6$	0.116	$4.47 \times 10^5$	-0.707
	1/8"	$2.77 \times 10^5$	0.257	$2.06 \times 10^4$	-0.379
	3/16"	$3.75 \times 10^4$	0.465	$4.25 \times 10^3$	-0.208

Table 1 summary of the results for Buna N and Viton 75 O-rings.

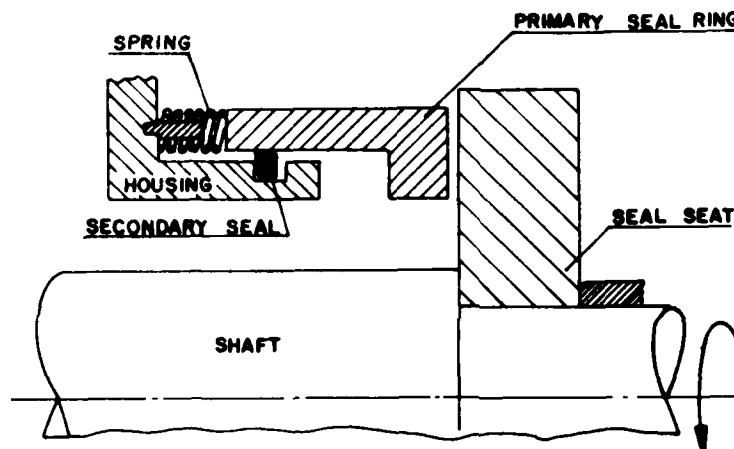


Fig. 1 Mechanical Face Seal

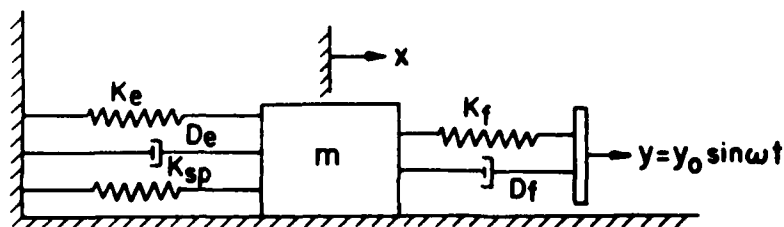


Fig. 2 Lumped parameters single degree of freedom model

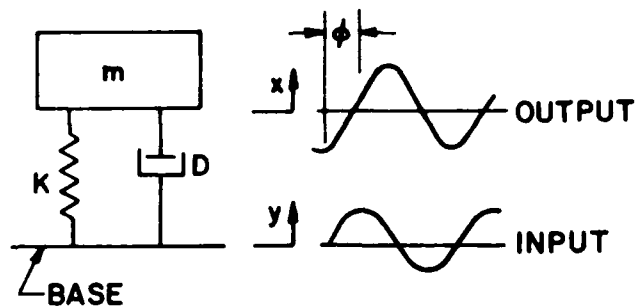


Fig. 3 Schematic of the BERM test method

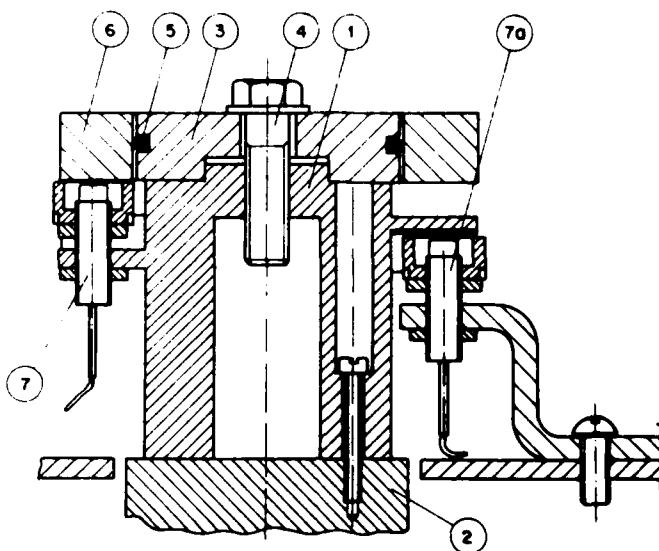


Fig. 4 Test rig for measuring O-rings dynamic properties

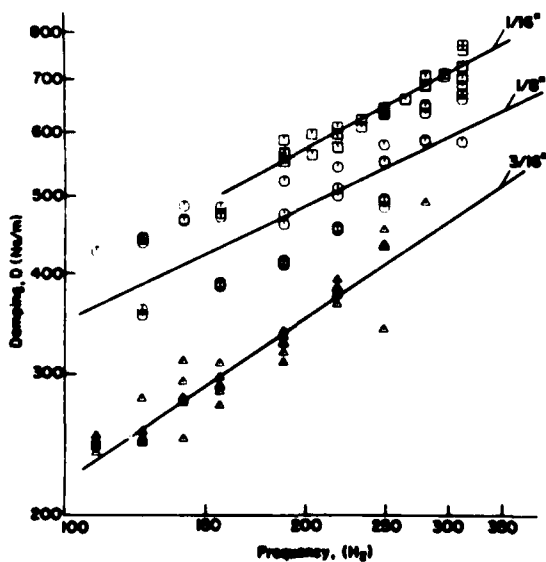


Fig. 5a Stiffness coefficient vs. frequency, Buna N

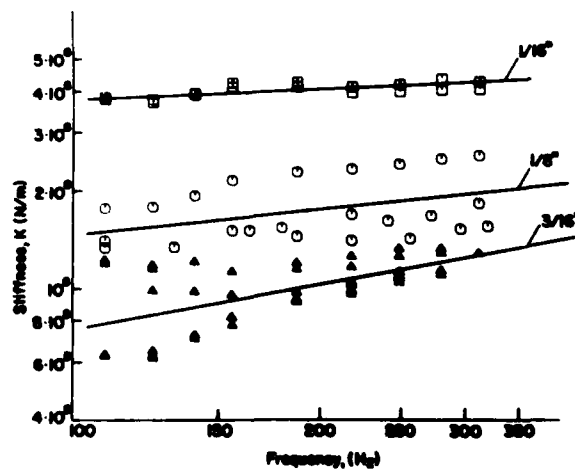


Fig. 5b Stiffness coefficient vs. frequency, Viton 75



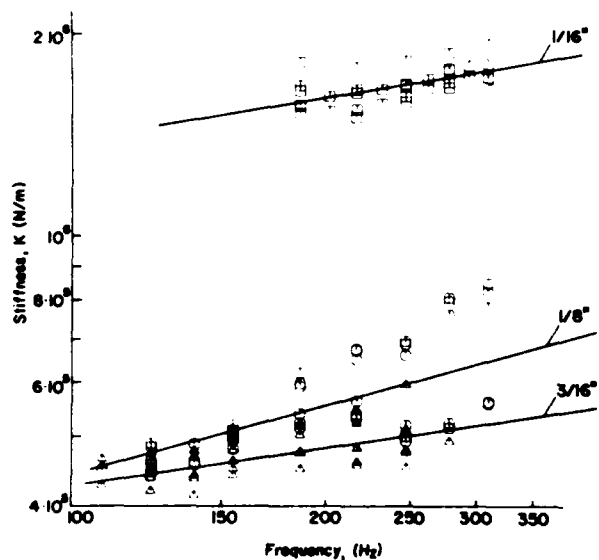


Fig. 6a Damping coefficient vs. frequency, Buna N

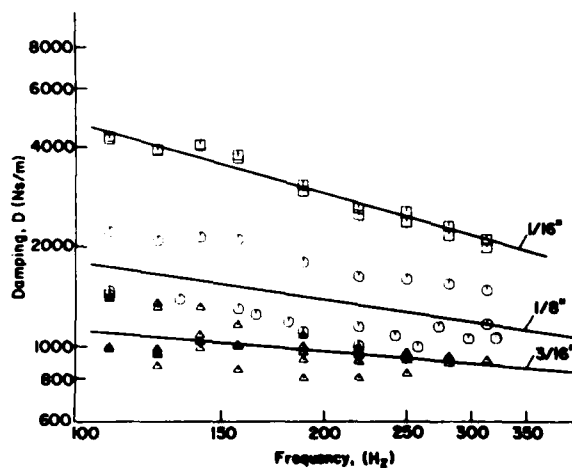


Fig. 6b Damping coefficient vs. frequency, Viton 75

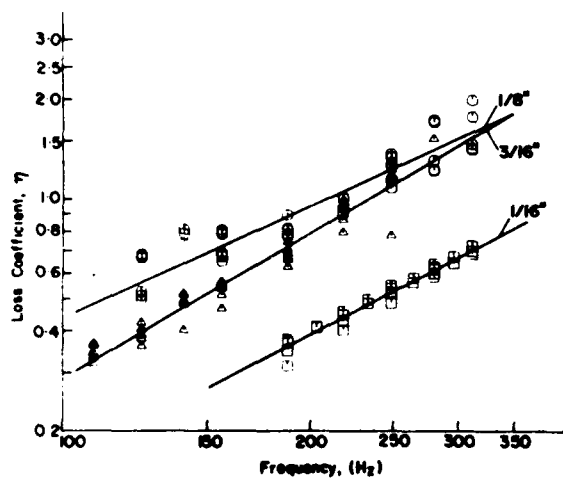


Fig. 7a Loss coefficient vs. frequency, Buna N

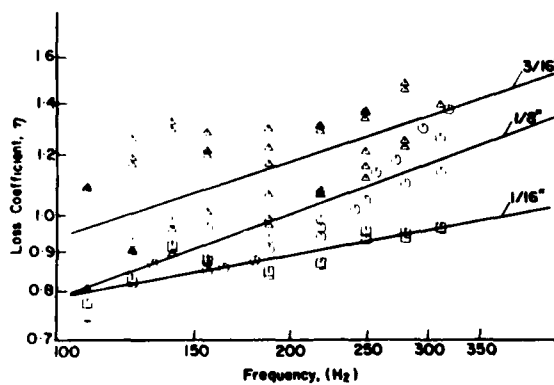


Fig. 7b Loss coefficient vs. frequency, Viton 75

APPENDIX B

A KINEMATIC MODEL FOR MECHANICAL SEALS WITH  
ANTIROTATION LOCKS OR POSITIVE DRIVE DEVICES

A KINEMATIC MODEL FOR  
MECHANICAL SEALS WITH ANTIROTATION  
LOCKS OR POSITIVE DRIVE DEVICES

by

I. Green and I. Etsion

EEC - 153

Dept. of Mechanical Engineering  
Technion, Haifa 32000, Israel

ISSN-0333-8045

June 1984

## ABSTRACT

A kinematic model of mechanical face seals is presented. Two basic seal arrangements are considered: A flexibly mounted stator with antirotation locks, and a flexibly mounted rotor with positive drive devices. The equation of kinematic constraint is derived and presented in a simple form for all the possible types of antirotation or positive drive mechanisms found in practical seals. This simple form is then used to derive the dynamic moments acting on the flexibly mounted element of the seal.

## NOMENCLATURE

$I$	transverse moment of inertia
$I_z$	polar moment of inertia
$\vec{L}$	relative angular momentum
$T$	transmission law
$\vec{T}$	dynamic moment
$\beta = -\psi$	
$\gamma$	nutation
$\vec{\lambda}$	absolute angular velocity
$\psi$	relative precession
$\psi_r$	absolute rotor precession
$\psi_s$	absolute stator precession
$\phi$	relative spin
$\omega$	shaft angular velocity
$\Omega$	relative angular velocity
$\omega_c$	reference angular velocity

## Subscripts

$r$	rotor
$s$	stator

## INTRODUCTION

Seal dynamics has become the subject of many investigations in the last decade [1]. Much effort is devoted to analyze the time-dependent behavior of the flexibly mounted element of the seal. This element can be either the rotating one, as in many low speed applications, or the stationary one as shown in Fig. 1. Its motion is affected by factors such as axial runout, shaft vibration, dynamic properties of both the flexible support and the lubricating fluid film, etc. These factors were considered in previous works [1,3,4] and the existing theoretical models are quite close to the realistic seals. There is, however, one aspect which was overlooked so far, but nevertheless plays an important role in seal dynamics. This is the constraint imposed on the flexibly mounted element by the positive drive devices in the case of a flexibly mounted rotor or by the anti-rotation locks (see Fig. 1) in the case of a flexibly mounted stator. Understanding of this constraint is essential for a correct formulation of the seal kinematics. Unfortunately, there are numerous different arrangements of positive drive or anti-rotation devices [5,6], e.g. dents, keys, pins, slots and ears, and bellows to name just a few. In addition, the number of units in a particular arrangement may vary in different designs, ranging, for example, from one to four pins per seal. Manufacturing tolerances regarding these devices are fairly large and therefore even in cases where several drives or locks are present, only one of them may actually be effective.

The constraint situation described above complicates any attempt to deal accurately with the kinematic model of mechanical seals. Such a model is, however, necessary for the derivation of the equations of motion. The present paper describes a general treatment that offers a fairly accurate solution to this complex problem. Based on the fact that the angular displacements of the flexibly mounted element are very small, it will be shown that a first order approximation serves as a good general model, with a truncation error of order  $\gamma^2$  where  $\gamma \ll 1$ . Finally, the dynamic moments that act upon the flexibly mounted element will be derived for the two basic arrangements where this element is either the rotor or the stator.

## THE KINEMATIC MODEL

Fig. 2 presents schematically a model of a mechanical face seal which assists in understanding the kinematics of the flexibly mounted seal element. The figure shows a system of two rings. An outer ring to which a reference XYZ is attached, and an inner ring with two slots to accommodate two pins that are fixed to the outer ring along the Y axis. The inner ring represents the flexibly mounted element of the seal and is free to have two orthogonal tilts about two of its diameters.

Two cases will be considered. 1) The flexibly mounted seal element is stationary, and 2) the flexibly mounted seal element is rotating. In the first case the outer ring represents the seal housing (see Fig. 1), the two pins represent the antirotation locks, and the reference XYZ is inertial. In the second case the outer ring represents the shaft, the two pins represent the positive drive mechanism and the reference XYZ, together with the outer ring, rotates at an angular velocity  $\omega$  about the Z axis.

The resultant of the two tilts of the inner ring can be described by the two Eulerian angles  $\gamma$  and  $\psi$  (see Fig. 2). The angle  $\gamma$  is the nutation of the inner ring about the axis x of a reference system xyz. This reference system is free to rotate with respect to the inner ring so that the axis y is always directed to the point of maximum distance from the XY plan. The angle  $\psi$  is the precession of the reference xyz with respect to the reference XYZ. The axis z of the rotating xyz reference coincides with the principal axis of the inner



ring. It is this axis about which the inner ring has a spin  $\phi$  with respect to the xyz reference.

An observer located in the reference xyz sees the reference XYZ and, hence, the outer ring rotating through an angle  $-\psi$  about axis Z while the inner ring rotates through an angle  $\phi$  about axis z. The kinematic constraint forces the two rings to complete one revolution simultaneously, while any pair of corresponding points on the circumference of the two rings return to their original relative positions after the completion of each revolution. This kinematic quality is characteristic of any universal joint and, hence, the seal model of Fig. 2 can be represented by a universal joint as shown in Fig. 3. Here, the rotation  $\beta = -\psi$  is the input to the joint related to the outer ring, and the rotation  $\phi$  is the output from the joint related to the inner ring.

The kinematic constraint represented by the two pins in Fig. 2 reduces the number of rotational degrees of freedom of the system into two, and dictates a certain relation between the Eulerian angles. This relation, known as the equation of kinematic constraint, has the general form

$$\phi = \phi(\gamma, \psi) \quad (1)$$

and is typical for universal joints (see for example the case of a Hooke Joint in [7] pp. 270-272).

As stated in the Introduction, numerous different arrangements of antirotation locks and positive drive mechanisms can be found in mechanical seals. Each one of these arrangements may result in a different particular form of eq. (1) making it impossible to derive a general kinematic formulation of the problem. This shortcoming can, however, be overcome by noting that the nutation angle  $\gamma$  in any practical seal is very small. Hence, for small  $\gamma$  the spin  $\phi$  in a general joint as shown in Fig. 3 can be expanded in the form

$$\phi = \phi_0 + \phi_1 \gamma + \phi_2 \gamma^2 + \dots \quad (2)$$

where  $\phi_i = \phi_i(\beta)$  are general periodic functions of  $\beta$ , and  $\beta = -\psi$ . For  $\gamma = 0$  we have  $\phi = \beta$ , hence

$$\phi_0 = \beta$$

Differentiating eq. (2) with respect to time yields

$$\dot{\phi} = \dot{\beta} + \frac{\partial \phi_1}{\partial \beta} \dot{\beta} \gamma + \phi_1 \dot{\gamma} + \frac{\partial \phi_2}{\partial \beta} \dot{\beta} \gamma^2 + 2\phi_2 \gamma \dot{\gamma} + \dots \quad (3)$$

The transmission law of the joint is thus given by

$$T = \frac{\dot{\phi}}{\dot{\beta}} = 1 + \frac{\partial \phi_1}{\partial \beta} \gamma + \phi_1 \frac{\dot{\gamma}}{\dot{\beta}} + \frac{\partial \phi_2}{\partial \beta} \gamma^2 + 2\phi_2 \gamma \frac{\dot{\gamma}}{\dot{\beta}} + \dots \quad (4)$$

For  $\gamma = 0$  any universal joint results in  $T = 1$ . Hence,

$$\phi_1 = 0$$

and the transmission law can be written as

$$T = 1 + \frac{\partial \phi_2}{\partial \beta} \gamma^2 + 2\phi_2 \gamma \frac{\dot{\gamma}}{\dot{\beta}} + \dots \quad (5)$$

For small perturbation, the order of  $\dot{\gamma}$  is the same as that of  $\gamma$ , and eq. (5) takes the form

$$T = \frac{\dot{\phi}}{\dot{\beta}} = 1 + O(\gamma^2) \quad (6)$$

Hence, for any practical mechanical seal where  $\gamma^2 \ll 1$  equation (6) gives the transmission,  $T$ , accurately enough, by  $T = 1$ .

In a Constant Velocity Joint the result  $T = 1$  is accurate independent of  $\gamma$ . This special case is characterized by the lack of preference to the order and direction of the two perpendicular tilts of the inner ring, and is typical, therefore, to such cases where the pins of Fig. 2 are either omitted or are not in effect. The first case corresponds to a flexible support that consists of a metal bellows. The second case occurs when the friction in the elastomeric secondary seal is sufficient to prevent rotation of the flexibly supported element.

As another example let us examine the case of a Hooke Joint. The equation of kinematic constraint for this particular joint is (see p. 272 in ref. (7)).

$$\tan \phi = \tan \beta \cos \gamma \quad (7)$$

Differentiating with respect to time and substituting  $\tan \phi$  from eq. (7), gives after some algebra

$$\dot{\phi} = \frac{\dot{\beta} \cos \gamma - \gamma \sin \gamma \sin \beta \cos \beta}{1 - \sin^2 \beta \sin^2 \gamma} \quad (8)$$

For small nutation angles,  $\gamma^2 \ll 1$ , we may use

$$\sin \gamma = \gamma$$

$$\cos \gamma = 1 - \frac{\gamma^2}{2}$$

so that

$$(1 - \sin^2 \beta \sin^2 \gamma)^{-1} = 1 + \gamma^2 \sin^2 \beta$$

Substituting these relations in eq. (8) and neglecting terms of order higher than  $\gamma^2$ , will finally give

$$\tau = \frac{\dot{\phi}}{\dot{\beta}} = 1 + (\sin^2\beta - \frac{1}{2})\gamma^2 - \frac{\gamma\dot{\gamma}}{\dot{\beta}} \sin\beta \cos\beta \quad (9)$$

Comparing corresponding terms in eqs. (9) and (4), we have

$$\phi_1 = \frac{\partial\phi_1}{\partial\beta} = 0$$

and

$$\frac{\partial\phi_2}{\partial\beta} = \sin^2\beta - \frac{1}{2}$$

which agrees with the fifth term in (4) that is

$$\phi_2 = -\frac{1}{2} \sin\beta \cos\beta$$

The particular form of eq. (2) for a Hooke Joint is therefore

$$\phi = \beta - \frac{\gamma^2}{2} \sin\beta \cos\beta \quad (10)$$

Recalling that  $\beta = -\psi$  and hence  $\dot{\beta} = -\dot{\psi}$  we may conclude that for any practical mechanical face seal, where  $\gamma^2 \ll 1$ , eq. (6) gives the spin  $\dot{\phi}$ , accurately enough, by

$$\dot{\phi} = -\dot{\psi} \quad (11)$$

## THE DYNAMIC MOMENTS

The term "dynamic moments" is used to describe the contribution of the inertia of a body to its behavior in the angular degrees of freedom. The rotational equations of motion of a body are formed by equating the dynamic moments with the "applied moments" that are contributed by external forces acting on the body. The correct formulation of the dynamic moments that act upon the flexibly mounted element of the seal is, therefore, essential for the two basic arrangements, the kinematics of which was analyzed in the previous section.

The general form of the dynamic moment vector of a rigid body expressed in a moving reference can be found in several texts, e.g. [7] and is given by

$$\vec{T} = \frac{\partial \vec{L}}{\partial t} + \vec{\omega}_c \times \vec{L} + \vec{r}_{go} \times m \vec{a}_o \quad (12)$$

where  $\vec{L}$  is the relative angular momentum vector of the rigid body defined as

$$\{L\} = [I] \{\lambda\} \quad (13)$$

and  $\vec{\lambda}$  is the absolute angular velocity vector of the body. The vector  $\vec{\omega}_c$  is the rotational velocity of the reference system accelerating at  $\vec{a}_o$ , and  $\vec{r}_{go}$  is the location of the center of mass of the body (in our model  $\vec{r}_{go} = 0$ ). The absolute angular velocity  $\lambda$  of the body is given by

$$\vec{\lambda} = \vec{\omega}_c + \vec{\Omega} \quad (14)$$

where  $\vec{\Omega}$  is the angular velocity vector of the body relative to the rotating reference.

In the seal model shown in Fig. 2 the body is the inner ring and the rotating reference is the xyz reference. Hence, due to the kinematic constraint  $\vec{\Omega}$  is always along the z axis and by definition is

$$\vec{\Omega} = \dot{\phi} \hat{z} \quad (15)$$

The spin  $\dot{\phi}$  is related to the precession  $\dot{\psi}$  by the equation of the kinematic constraint, which for small nutation  $\gamma$  is given in eq. (11).

Flexibly Mounted Stator: The angular velocity of the rotating reference for this case is (see Fig. 2)

$$\vec{\omega}_c = \dot{\gamma}_s \hat{x} + \dot{\psi}_s \sin \gamma_s \hat{y} + \dot{\psi}_s \cos \gamma_s \hat{z} \quad (16)$$

Where the subscript s is used to indicate the stator as the flexibly mounted element. Substituting eqs. (16), (15) and (11) in eq. (14) we have for the angular absolute velocity of the stator

$$\vec{\lambda}_s = \dot{\gamma}_s \hat{x} + \dot{\psi}_s \sin \gamma_s \hat{y} + \dot{\psi}_s (\cos \gamma_s - 1) \hat{z} \quad (17)$$

Hence, by eq. (13) the relative angular momentum vector L is

$$\vec{L}_s = I \dot{\gamma}_s \hat{x} + I \dot{\psi}_s \sin \gamma_s \hat{y} + I_z \dot{\psi}_s (\cos \gamma_s - 1) \hat{z} \quad (18)$$

where  $I_z$  is the polar moment of inertia, and  $I = I_x = I_y$  is the transverse moment of inertia of the flexibly mounted element.

Using eqs. (18) and (16) in eq. (12), recalling that  $\vec{r}_{go} = 0$ , and that we are dealing with small angles  $\gamma$  so that  $\cos\gamma_s = 1$  and  $\sin\gamma_s = \gamma_s$  are valid approximations, we have the dynamic moments in the form

$$T_x = I(\ddot{\gamma}_s - \dot{\psi}_s^2 \gamma_s) \quad (19a)$$

$$T_y = I(\ddot{\psi}_s \gamma_s + 2\dot{\psi}_s \dot{\gamma}_s) \quad (19b)$$

$$T_z = -I_z(\dot{\psi}_s \dot{\gamma}_s \gamma_s + \ddot{\psi}_s \gamma_s^2/2) \quad (19c)$$

As can be seen from eq. (19c) the dynamic moment  $T_z$  is of order  $\gamma^2$  and hence, can be neglected in any practical seal.

Flexibly Mounted Rotor: In this case the outer ring in Fig. 2 which represents the shaft has an angular velocity  $\omega$ . This velocity when added to the relative precession  $\dot{\psi}$  of the rotating reference xyz gives the absolute precession of the rotor,  $\dot{\psi}_r$ , in the form

$$\dot{\psi}_r = \dot{\psi} + \omega \quad (20)$$

where the subscript r is used to indicate the rotor as the flexibly mounted element.

From eqs. (11) and (20) we have

$$\dot{\phi} = \omega - \dot{\psi}_r \quad (21)$$

The angular velocity  $\vec{\omega}_c$  of the reference XYZ is given by eq. (16) where the subscript s is replaced everywhere by the subscript r. Similarly, the absolute angular velocity of the inner ring is given by eq. (14) where  $\vec{\Omega}$  is given in (15) and  $\dot{\phi}$  in (21).

Hence,

$$\vec{\lambda}_r = \dot{\gamma}_r \hat{x} + \dot{\psi}_r \sin \gamma_r \hat{y} + [\dot{\psi}_r (\cos \gamma_r - 1) + \omega] \hat{z} \quad (22)$$

The relative angular momentum vector  $\vec{L}$  is

$$\vec{L}_r = I \dot{\gamma}_r \hat{x} + I \dot{\psi}_r \sin \gamma_r \hat{y} + I_z [\dot{\psi}_r (\cos \gamma_r - 1) + \omega] \hat{z} \quad (23)$$

and the dynamic moments have, by (12), the form

$$T_x = I(\ddot{\gamma}_r - \dot{\psi}_r^2 \gamma_r) + I_z \omega \dot{\psi}_r \gamma_r \quad (24a)$$

$$T_y = I(\ddot{\psi}_r \gamma_r + 2\dot{\psi}_r \dot{\gamma}_r) - I_z \omega \dot{\gamma}_r \quad (24b)$$

$$T_z = -I_z(\dot{\psi}_r \dot{\gamma}_r \gamma_r + \ddot{\psi}_r \gamma_r^2/2) \quad (24c)$$

Here again  $T_z$  is of order  $\gamma^2$  and can be neglected in practical seals.



## SUMMARY AND CONCLUSION

The kinematic model of mechanical face seals was presented. Two basic seal arrangements were considered. These are the flexibly mounted stator and the flexibly mounted rotor. The kinematic constraint provided by the antirootation locks in the first arrangement or by the positive drive devices in the second was shown to be similar to that of a universal joint. It was shown that inspite of the numerous variations of antirootation locks and positive drive mechanisms found in mechanical seals, it is possible to present the equation of kinematic constraint in the simple form

$$\dot{\phi} = -\dot{\psi}$$

This unified relation is the result of the very small nutation,  $\gamma$ , in practical seals, and is accurate to an order  $\gamma^2$  where  $\gamma \ll 1$ .

The simple general form of the equation of kinematic constraint enables to derive the dynamic moments that act on the flexibly mounted seal element. These moments are presented in eqs. (19) for the case of a flexibly mounted stator, and in eqs. (24) for the case of a flexibly mounted rotor. In both cases the dynamic moment  $T_z$  which is the axial component of the moment vector was found negligible. The two other components, namely  $T_x$  and  $T_y$  depend on the transverse moment of inertia,  $I$ , in the the case of a flexibly mounted stator, and on both the transverse and polar moments of inertia,  $I$  and  $I_z$  in the case of the flexibly mounted rotor. The contribution of the polar moment of inertia in seals with flexibly mounted rotor alters the dynamic moments  $T_x$  and  $T_y$  as com-

pared to the flexibly mounted stator case. This is equivalent to altering the inertia of the flexibly mounted element and may affect the dynamic behavior.

The analysis presented in this paper assumed no more than two pins as a representation of the constraint provided by the antirotation locks or positive drive devices. If three or more units are effective, then the inner ring is actually "locked" and is unable to track angular misalignment of the rigidly mounted element. Such a condition can be avoided by limiting the number of antirotation locks and positive drive devices in a seal to two units at most.

#### Acknowledgement

The research reported here was supported in parts by the Israel Academy of Sciences and the U.S. Air Force Wright Aeronautical Laboratories/AFWAL/POSL under contract F49620-83-C-0057.

## References

1. Etsion, I., "A Review of Mechanical Face Seal Dynamics". The Shock and Vibration Digest, Vol. 14, No., 3, March 1982, pp. 9-14.
2. Nau, B.S., "Vibration and Rotary Mechanical Seals", Tribology International, Feb. 1981 pp. 55-59.
3. Green, I., and Etsion, I., "Fluid Film Dynamic Coefficients in Mechanical Face Seals", Trans. ASME Jour. of Lub. Tech., Vol, 105, No. 2, April 1983, pp. 297-302.
4. Green, I., and Etsion, I., "Stiffness and Damping Characteristics of Elastomer O-rings Secondary Seals Subjected to Reciprocating Twist", Proc. 10th International Conf. on Fluid Sealing, BHRA, April 1984. (see Appendix A)
5. Buchter, H.H., "Industrial Sealing Technology", John Wiley & Sons, Inc., 1979.
6. Crane Packing Company, "Engineered Fluid Sealing", 1976.
7. Arnold, N.R., and Maunder, L., "Gyrodynamics and its Engineering Applications", Academic Press, New York, 1961.

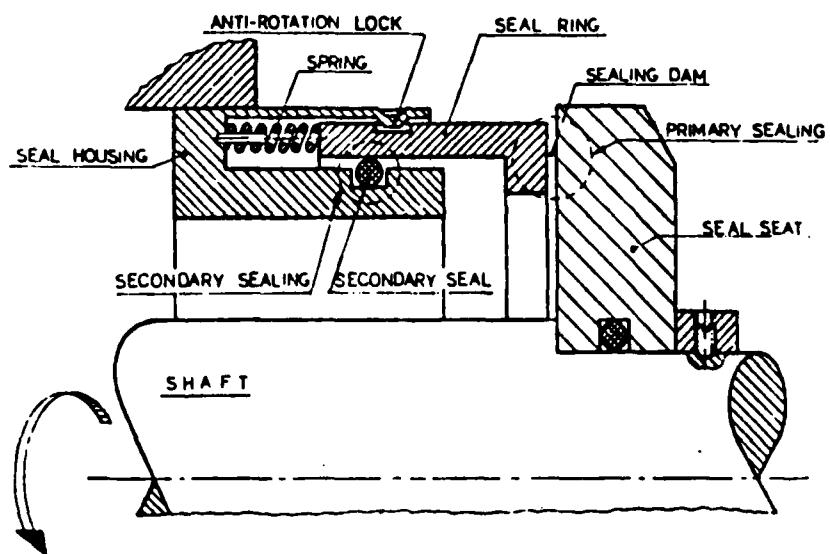


Fig. 1 Mechanical face seal - schematic and terminology

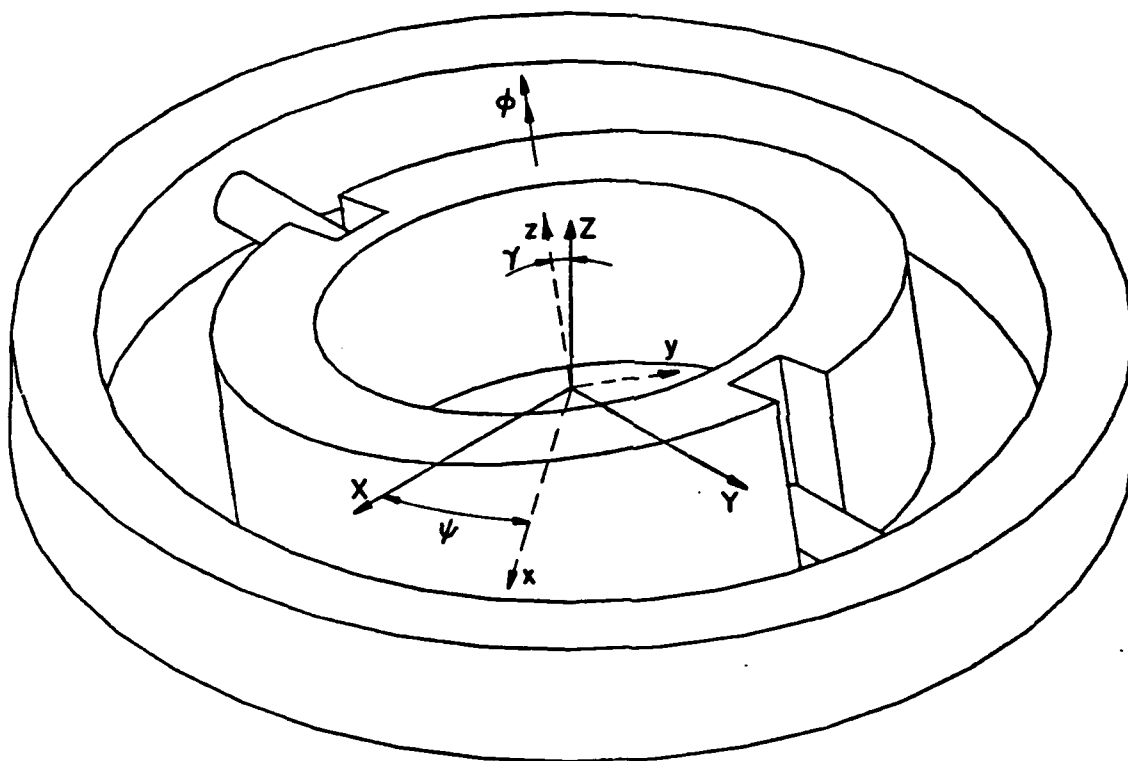


Fig. 2 Seal kinematic model.

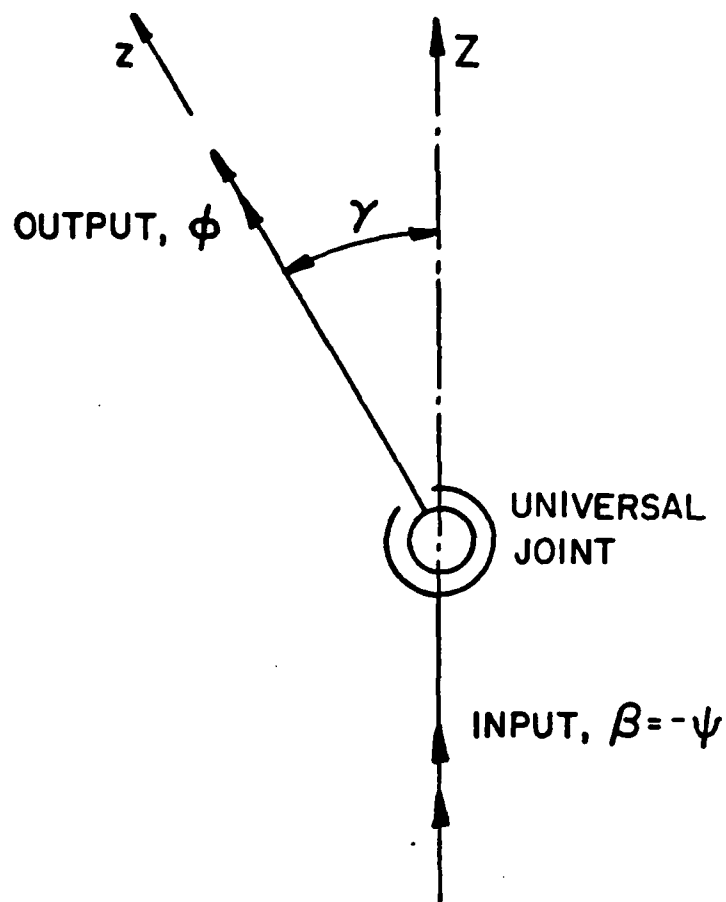


Fig. 3 Universal Joint model.

APPENDIX C  
STABILITY THRESHOLD AND STEADY-STATE RESPONSE  
OF NONCONTACTING CONED-FACED SEALS



# Stability Threshold and Steady-State Response of Noncontacting Coned-Face Seals<sup>©</sup>

I. GREEN and I. ETSION (Member, ASLE)  
Technion, Haifa 32000, Israel

*The dynamic behavior of a noncontacting coned-face seal is analyzed. Stiffness and damping properties of the fluid film and flexible support including elastomeric secondary seal are fully accounted for. Stability threshold and steady-state response in the presence of rotor axial runout and assembly misalignment are investigated. An expression is provided for the critical speed above which the seal becomes dynamically unstable. For stable operation,*

*the relative misalignment between the mating faces is given as a function of rotor runout, assembly misalignment, design parameters, and operation conditions. An expression is provided for the critical rotor runout above which the seal will fail due to face contact. Although the analysis is based on small perturbation assumption, it is shown to be valid in many practical cases.*

Presented as an American Society of Lubrication Engineers paper at the ASLE/ASME Lubrication Conference in San Diego, California, October 22-24, 1984  
Final manuscript approved May 30, 1984

## NOMENCLATURE

$C$  = centerline clearance  
 $C_d$  = design clearance  
 $D^*$  = damping coefficient  
 $D$  = dimensionless damping coefficient; angular  $D^*_1 \omega C_d / Sr_o^3$ , axial  $D^*_2 \omega C_d / Sr_o^3$   
 $F^*$  = force  
 $F$  = dimensionless force  $F^* / Sr_o^2$   
 $H$  = dimensionless film thickness,  $h/C$   
 $h$  = local film thickness  
 $I^*$  = stator moment of inertia  
 $I$  = dimensionless moment of inertia,  $I^* \omega^2 C_d / Sr_o^3$   
 $K^*$  = stiffness coefficient  
 $K$  = dimensionless stiffness coefficient; angular  $K^*_1 C_d / Sr_o^3$ , axial  $K^*_2 C_d / Sr_o^3$   
 $M^*$  = moment  
 $M$  = dimensionless moment,  $M^* / Sr_o^3$   
 $M_{\gamma_i}$  = dimensionless moment due to stator initial misalignment  
 $M_{\gamma_r}$  = dimensionless moment due to rotor runout  
 $m^*$  = stator mass  
 $m$  = dimensionless mass,  $m^* \omega^2 C_d / Sr_o^3$   
 $P$  = dimensionless pressure,  $p/S$   
 $p$  = pressure  
 $R$  = dimensionless radial coordinate,  $r/r_o$   
 $r$  = radial coordinate  
 $S$  = seal parameter,  $6\mu\omega(r_o/C_d)^2 (1-R_o)^2$   
 $t$  = time  
 $Z$  = axial degree of freedom

$\beta^*$  = face coning  
 $\beta$  = dimensionless coning,  $\beta^* r_o / C_d$   
 $\gamma^*$  = relative misalignment  
 $\gamma$  = dimensionless misalignment,  $\gamma^* r_o / C_d$   
 $\gamma_o$  = dimensionless relative misalignment caused by rotor runout alone  
 $\gamma_r$  = dimensionless rotor runout  
 $(\gamma_r)_c$  = dimensionless critical rotor runout  
 $\gamma_i$  = dimensionless tilt of the stator  
 $\gamma_{oi}$  = dimensionless stator initial misalignment  
 $\gamma_{oi}$  = dimensionless steady-state stator response due to  $\gamma_{oi}$  alone  
 $\gamma_{or}$  = dimensionless steady-state stator response due to  $\gamma_r$  alone  
 $\theta$  = angular coordinate  
 $\mu$  = viscosity  
 $\xi$  = damping ratio  
 $\psi$  = precession  
 $\omega$  = shaft angular velocity

## Subscripts

$cr$  = critical  
 $d$  = dynamic (velocity) effect  
 $e$  = elastomer  
 $f$  = fluid film  
 $i$  = inner radius  
 $m$  = mid radius  
 $o$  = outer radius  
 $r$  = rotor  
 $s$  = stator, or flexible support  
 $sp$  = springs



Only recently has dynamics become the subject of theoretical investigations and more rigorous experimentation. Reference (1) covers the literature until 1981 while Refs. (2)–(4) present more recent results on the subject.

The basic seal model, as shown in Fig. 1, has one fixed component that is rigidly mounted either to the shaft or to the housing (in Fig. 1 the rigidly mounted component is the rotor). The other component is flexibly mounted to allow tracking of various misalignments. These misalignments can be the result of manufacturing or assembly tolerances. Thus, in the seal of Fig. 1, for example, the rotor may have a certain axial runout and the stator too, may be misaligned to the shaft due to imperfections in its flexible support. In fact, it is very unlikely to have any perfect alignment at all in practical seals. In operation, the rotor wobbles because of its runout and this motion is transmitted via the fluid film to the stator. The dynamic characteristics of the system (namely, stiffness and damping of both the fluid film and flexible support, as well as the inertia of the stator) will determine the dynamic behavior of the seal. The stator can become completely unstable or it can track the rotor runout in a dynamically stable mode. However, even in this stable mode, the combination of tracking amplitude and phase shift can be such that the relative position between stator and rotor results in seal failure. Such a failure can be either due to excessive leakage caused by large gaps, or due to local face contact in high-speed noncontacting seals.

In previous works on seal dynamics, e.g. (5), (6), some simplifying assumptions were made which restricted the results but nevertheless gave good insight of the problem. The restricting assumptions include neglect of various fluid film effects, neglect of rotor and stator misalignments, and neglect or incomplete information on the dynamic properties of the flexible support. In this paper, a dynamic analysis of coned-face seals is presented which takes into account many factors that affect the seal dynamics. These factors are the rotor runout, initial misalignment of the stator before attachment to the rotor, coning of the stator, stiffness and damping of the fluid film, and stiffness and damping of the flexible support. Two assumptions will be made, however, to enable closed-form analytical solution. It will be assumed that (1) the seal is only slightly perturbed from the position of parallel faces, and (2) that the stator amplitude is small enough to prevent slippage of the secondary seal.

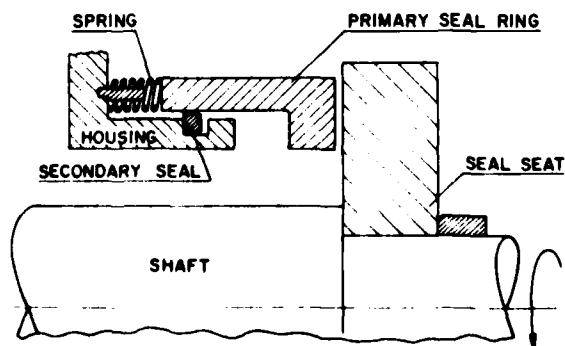


Fig. 1—Schematic of a radial face seal

The first assumption seems at first to be very restrictive. However, it will be shown by a numerical example that this is the case in most practical applications. The second assumption is valid for many practical cases and permits representation of elastomeric secondary seals by relatively simple to handle dynamic coefficients.

Although the present analysis is performed for a coned-face seal with an elastomeric O-ring secondary seal, the results will be presented in terms of general dynamic coefficients and, hence, are applicable to other noncontacting seal types as well.

## SYSTEMS OF COORDINATES AND GENERALIZED FORCES

The seal model and various coordinate systems are shown in Fig. 2. The inertial reference  $XYZ$  is fixed in space and its axis  $Z$  coincides with the shaft axis of rotation. The system  $xyz$  defines the relative position of the stator with respect to the inertial reference. This system is located in the stator plane but is free to rotate so that axis  $y$  always points to the point of maximum distance from the plane  $XY$ , and axis  $x$  is always parallel to the  $XY$  plane. The angle  $\psi$ , between axes  $X$  and  $x$ , is the precession and the angle  $\gamma^*$  is the nutation defining the angular tilt of the stator with respect to the inertial reference. The system  $x_r y_r z_r$  is fixed to the rotor and rotates with it at the angular velocity  $\omega$  about the  $Z$  axis. Axis  $x_r$  is always parallel to the  $XY$  plane making an angle  $\omega t$  with the  $X$  axis. Axis  $y_r$  always points to the point of minimum distance from the  $XY$  plane. The angle  $\gamma_r^*$  represents the runout of the rotor. Because the separation

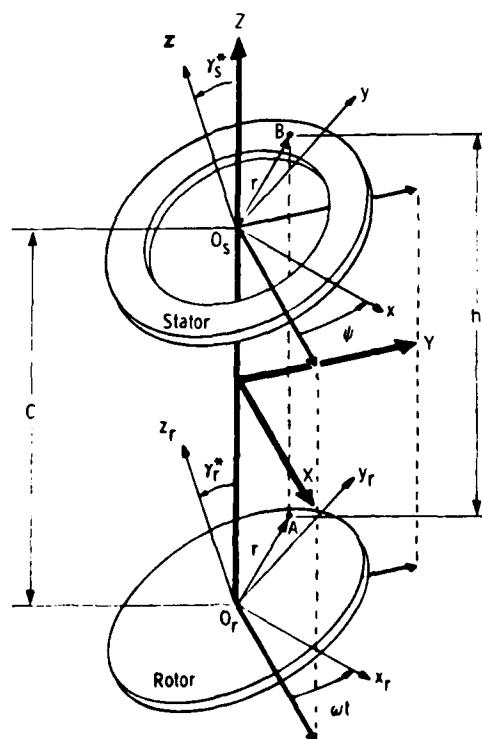


Fig. 2—Seal model and coordinate systems

$C$  between the stator and rotor is very small (a few micrometers in practical applications)  $\gamma^*$  and  $\gamma_r^*$  are also very small and can be treated as vectors. Hence, the relative misalignment between the stator and rotor is

$$\gamma^* = \gamma_r^* - \gamma_s^* \quad [1]$$

Figure 3 shows the relative position between the stator (seal ring) and rotor (seal seat). This relative position is described by a new coordinate system 123. This system is free to rotate within the stator plane so that axis 1 (about which the stator relative tilt  $\gamma^*$  takes place) is always parallel to the rotor plane and axis 2 always points to the point of maximum film thickness.

The various coordinate systems and a vector representation of the tilts  $\gamma$ ,  $\gamma_s$ , and  $\gamma_r$  about the axes 1,  $x$ , and  $x_r$ , respectively, are shown in Fig. 4. The angle  $\phi$  is measured from the plane  $ZY$  to the plane  $O, O, AB$  in Fig. 2. The angle  $\theta$  is measured in the stator plane from axis 2 to the line  $OB$ . Hence, the local film thickness measured between points  $A$  and  $B$  in Fig. 2 is

$$h = C + \gamma^* r \cos \theta + \beta^*(r - r_0) \quad [2]$$

where

$$\theta = \phi - \phi_1 \quad [3]$$

and  $\phi_1$  is the angle between axes  $X$  and 1 or alternatively between axes  $Y$  and 2. Equation [2] takes account of stator coning as shown in Fig. 3 where  $\beta^*$  is the coning angle.

The wobbling motion of the rotor due to its runout, and the relative misalignment,  $\gamma$ , between stator and rotor produce a system of fluid film forces and moments which is

applied to the stator. The flexible support of the stator which consists of springs and a secondary seal (usually an elastomeric ring) produce another system of forces and moments that act on the stator. In linear systems, the sum of the applied forces in degree of freedom  $j$  due to a disturbance in degree of freedom  $i$  can be expressed in the general form

$$\sum F_j = - \sum_i (K_{ij} x_i + D_{ij} \dot{x}_i) \quad [4]$$

where  $F_j$  is a generalized force (a force or a moment) and,  $K_{ij}$  and  $D_{ij}$  are stiffness and damping coefficients, respectively. In our case (where for small perturbations the system can be considered linear), both the fluid film and the flexible support contribute stiffness and damping. Hence, the stiffness  $K$  is

$$K = K_f + K_s \quad [5a]$$

where the support stiffness  $K_s$  includes the contributions of the springs and the elastomeric secondary seal. Thus,

$$K_s = K_{sp} + K_r$$

The damping  $D$  is

$$D = D_f + D_s \quad [5b]$$

where in many practical cases the only source for the support damping  $D_s$  is the elastomer, in which case  $D_s = D_r$ .

Fluid film stiffness and damping coefficients for a coned-face seal were analyzed in (7) and are summarized in Table 1. These coefficients are conveniently calculated in the

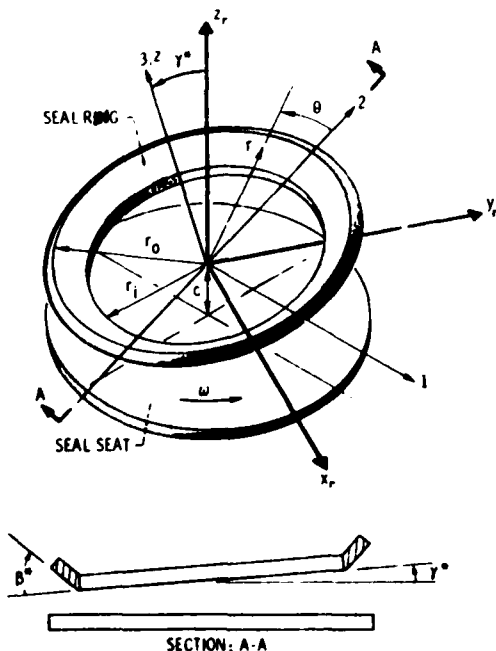


Fig. 3—Relative position between seal ring and seal seat

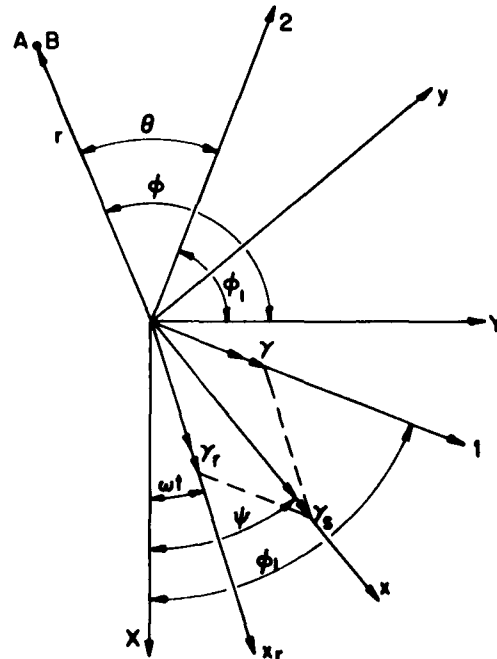


Fig. 4—Vector representation of the tilts  $\gamma$ ,  $\gamma_s$ ,  $\gamma_r$

TABLE 1—NONDIMENSIONAL FLUID FILM STIFFNESS AND DAMPING COEFFICIENTS  $K_f$  AND  $D_f$ 

		$j = 1$	$j = 2$	$j = 3$
$i = 1$	$K$	$\pi(P_o - P_i)(\beta R_i - 1)E_o^2$	$2\pi R_m^3 G_o \left( \dot{\phi}_1 - \frac{1}{2} \right)$	0
	$D$		0	
$i = 2$	$K \text{ \& } D$	0	0	0
$i = 3$	$K$	0	0	$\pi(P_o - P_i) \frac{2\beta}{R_m} E_o^2$
	$D$			$4\pi R_m G_o$

$$E_o = \frac{(1 - R_i) R_m}{2 + \beta(1 - R_i)}$$

$$G_o = \frac{\{n[1 + \beta(1 - R_i)] - 2\} \frac{\beta(1 - R_i)}{2 + \beta(1 - R_i)}}{\beta^3(1 - R_i)^2}$$

$$G_{o_{\text{avg}}} = \frac{1 - R_i}{12}$$

coordinate system 123 of Fig. 3 and, for the small perturbation case, are linear. It should be noted, however, that the dynamic coefficients presented in Table 1 were found valid even beyond the range of small perturbations (7).

Dynamic properties of elastomeric O-ring secondary seals were investigated in (8). In the absence of slippage, their stiffness and damping coefficients can be expressed in the form

$$K_f = A\omega^B$$

and

$$D_f = a\omega^b$$

where the coefficients  $A, B, a, b$  depend on factors such as material composition, temperature, ring dimension, pre-load etc.

In obtaining the system of forces and moments applied by the flexible support, it is useful to observe the various stages of seal assembling as shown in Fig. 5. Before any attachment takes place [Fig. 5(a)], the rotor has its runout  $\gamma_r$  and the stator has a certain initial misalignment  $\gamma_o$ . During the assembly, the stator is pressed against the rotor. This can be described by first tilting the stator by the amount  $\gamma_o$  [Fig. 5(b)] which requires a moment  $M_{X_0}$  given by

$$M_{X_0} = K_{X_0} \gamma_o \quad [6]$$

where  $K_{X_0}$  is the angular stiffness of the flexible support (see Appendix I). The initial tilt of the stator was selected arbitrarily in the opposite direction of the inertial axis  $X$  without losing the generality of the analysis. Since  $\gamma_o$  is fixed both in magnitude and direction, the moment  $M_{X_0}$  of Eq. [6] is also fixed in magnitude and direction (which is along the  $X$  axis).

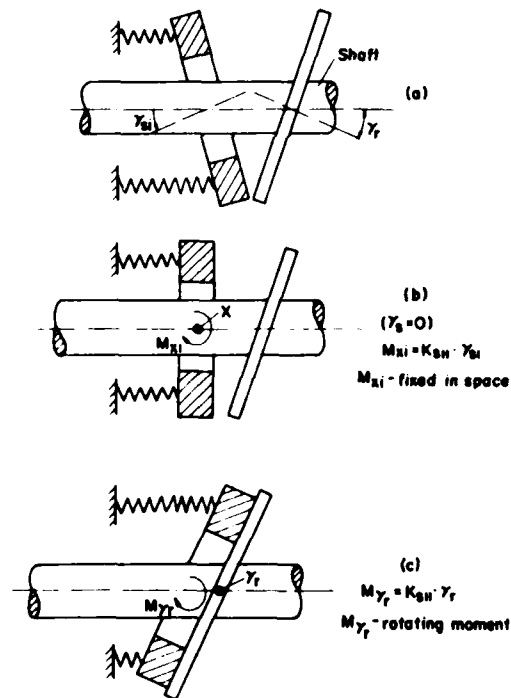


Fig. 5—Description of initial misalignments and attachment sequence of the seal components.

Final attachment of the seal mating faces in the assembling process [Fig. 5(c)] results in an additional moment that is required to tilt the stator by the amount of the rotor runout. Hence,

$$M_{Y_r} = K_{Y_r} \gamma_r \quad [7]$$

The moment  $M_{\omega}$ , like the runout  $\gamma_r$ , has a fixed magnitude but is rotating at the shaft speed  $\omega$ , and is directed along the axis  $x$ , (Fig. 4).

The moments acting on the stator during operation and resulting from the flexible support are given in the system  $xyz$  of Fig. 4 in the form

$$M_{yx} = -K_{y11}\gamma_y - D_{y11}\dot{\gamma}_y \quad [8a]$$

$$M_{\alpha\gamma} = -D_{\alpha\beta\gamma}\dot{\psi}\gamma_\beta \quad [8b]$$

Fluid film moments expressed in terms of the fluid film stiffness and damping coefficients (7) are given in the reference system 123 by

$$M_{ll} = -K_{ll}\gamma - D_{ll}\dot{\gamma} \quad [9a]$$

$$M_{f2} = -D_{f11} \left( \dot{\Phi}_1 - \frac{1}{g} \right) \gamma \quad [9b]$$

The complete system of moments acting on the stator is shown in the vectors diagram of Fig. 6. With the aid of this figure, there is no difficulty in describing the moments in any convenient reference system like the inertial system  $XYZ$  or the rotating system  $xyz$ .

The net axial force along the  $Z$  axis is given by

$$F_z = -K_{33}Z - D_{33}\dot{Z} \quad [10]$$

## SEAL RING STABILITY

In the following, dimensional parameters will be indicated by an asterisk to distinguish them from their corresponding dimensionless values. Also, the subscript 11 will be omitted from the angular stiffness and damping coefficients. Hence, whenever  $K$  and  $D$  will be used without any index they will correspond to angular degree of freedom. Only the subscript 33 will be retained for the axial degree of freedom.

The equation of motion in the axial degree of freedom is by [10] and [68] of Appendix 2:

$$m\ddot{Z} + D_{33}\dot{Z} + K_{33}Z = 0 \quad [11]$$

This equation is linear and uncoupled with the equations of motion in the angular degrees of freedom. Its solution is

$$Z = Z_0 e^{\lambda t}$$

resulting in the characteristic equation

$$m\lambda^2 + D_{33}\lambda + K_{33} = 0 \quad [12]$$

The condition for stable operation in the axial mode requires that all the coefficients of [12] will be positive. The dimensionless mass  $m$  and support damping  $D_{33}$  are always positive. The damping  $D_{43}$  is

$$D_{33} = D_{,33} + D_{/33}$$

and since  $D_{f33} > 0$  (see Table 1),  $D_{33}$  is also always positive. Hence, in order to satisfy the stability condition, it remains to require that  $K_{33} > 0$ . Substituting  $K_{f33}$  from Table 1 in [5a], we have

$$\pi(P_o - P_i) \frac{2\beta}{R_\pi} E_o^2 + K_{133} > 0 \quad [13]$$

Condition [13] is satisfied whenever  $\beta = 0$  (corresponding to a face seal). With coned face, axial stability is always obtained when the film converges in the direction of pressure drop.

To analyze the angular stability, the linear equations [66] and [67] of Appendix 2 are used. For the transient response, only the homogeneous part of these equations has to be considered, namely

$$I\dot{\gamma}_X + D\dot{\gamma}_X + K\gamma_X + \frac{1}{2}D_I\gamma_W = 0 \quad [14a]$$

$$I\ddot{\gamma}_Y + D\dot{\gamma}_Y + K\gamma_Y + \frac{1}{2}D_I\dot{\gamma}_X = 0 \quad [14b]$$

Using complex notation, the relation between the stator tilt  $\gamma$ , and its components  $\gamma_x$  and  $\gamma_y$  can be represented in the form (see Fig. 4)

$$\gamma_i = \gamma_x + i\gamma_y \quad [15]$$

where

$$1 - \sqrt{-1}$$

Multiplying Eq. [14b] by  $r$  and adding it to Eq. [14a], noting that

$$\gamma_x = \gamma_{xy} - \gamma_y$$



**Fig. 6—Vector representation of tilts and moments**

yields

$$I\gamma_c + D\dot{\gamma}_c + K\gamma_c - i\frac{1}{2}D_f\gamma_c = 0 \quad [16]$$

The complex term  $-i\frac{1}{2}D_f\gamma_c$  in Eq. [16], induced by hydrodynamic effects in the fluid film, represents a transverse moment which leads the displacement  $\gamma_c$  by  $\pi/2$  radians.

The solution of Eq. [16] is of the form

$$\gamma_c = \gamma_0 e^{i\lambda t} \quad [16a]$$

and the complex characteristic equation is

$$I\lambda^2 + D\lambda + K - iB = 0 \quad [17]$$

where

$$B = D_f/2$$

Multiplying Eq. [17] by its conjugate form gives the characteristic equation for the angular mode in its real form

$$I^2\lambda^4 + 2ID\lambda^3 + (2IK + D^2)\lambda^2 + 2DK\lambda + (K^2 + B^2) = 0 \quad [18]$$

The necessary condition for stability requires that all the coefficients in [18] will be positive. The dimensionless moment of inertia  $I$  is always positive. From [5b] and Table 1, it can be seen that  $D > 0$ . Hence, angular stability requires that

$$2IK + D^2 > 0 \quad [19a]$$

and

$$2DK > 0 \quad [19b]$$

Conditions [19a] and [19b] are satisfied whenever  $K > 0$ . Thus, from Eq. [5a] and Table 1, the necessary condition for angular stability is

$$\pi(P_o - P_i)(\beta R_s - 1)E_o^2 + K_s > 0 \quad [20]$$

Defining a critical coning angle  $\beta_{cr} = 1/R_s$ , it is seen from [20] that for  $P_o > P_i$  angular stability is assured whenever  $\beta > \beta_{cr}$ . In Ref. (7), an optimum coning angle for maximum angular stiffness  $K_f$  was found in the form  $\beta_{opt} = 2/R_s(1 - R_s)$ . It is clear that this  $\beta_{opt}$  is larger than  $\beta_{cr}$  and, hence, an optimum coning angle assures the fulfillment of condition [20] whenever  $P_o > P_i$ .

The Routh-Hurwitz stability criterion for Eq. [18] requires, in addition to fulfilling condition [20], that the four following conditions are also met:

$$2ID > 0 \quad [21a]$$

$$2I^2DK + 2ID^3 > 0 \quad [21b]$$

$$4ID^2(KD^2 - IB^2) > 0 \quad [21c]$$

$$4ID^2(K^2 + B^2)(KD^2 - IB^2) > 0 \quad [21d]$$

Since  $I$  and  $D$  are positive and fulfillment of condition [20] means that  $K$  is positive too, it remains to require that

$$KD^2 - IB^2 > 0$$

Hence, the angular stability threshold corresponds to the case

$$KD^2 - IB^2 = 0 \quad [22]$$

Substituting  $B = D_f/2$  and rearranging Eq. [22] gives the dimensionless critical moment of inertia in the form

$$I_{cr} = 4(K_f + K_s)\left(1 + \frac{D_s}{D_f}\right)^2 \quad [23a]$$

In Ref. (6), an empirical stability threshold was found for the case  $D_s = 0$  from a vast number of numerical solutions without the restriction of small perturbations. The critical moment of inertia in (6) has the form

$$I_{cr} = 4(K_s + R_s^2 K_f) \quad [23b]$$

where  $K_f$  has the value of the fluid film coefficient  $K_{f11}$  of Table 1. As can be seen,  $I_{cr}$  of [23b] is very similar to that of [23a] when  $D_s = 0$ , especially for narrow seals where  $R_s$  is close to unity.

Replacing the dimensionless parameters in Eq. [23a] with their corresponding dimensional parameters (see nomenclature) yields a dimensional critical speed  $\omega_{cr}$  in the form

$$\omega_{cr}^2 = 4 \frac{K_f^* + K_s^*}{I^*} \left(1 + \frac{D_s^*}{D_f^*}\right)^2 \quad [24]$$

For angular stability, the operation speed  $\omega$  should be smaller than  $\omega_{cr}$ . As can be seen from [24], an increase of the stiffness and reduction of the inertia increases the critical speed as expected. However, increasing the fluid film damping  $D_f^*$  reduces  $\omega_{cr}$ . This is due to the hydrodynamic effect (represented by  $D_f^*$ ) which results in a transverse moment leading the stator tilt by  $\pi/2$  (see Eq. [16]). Since  $K_f^*$  is directly proportional to the pressure differential  $p_o - p_i$ , and  $D_f^*$  is directly proportional to the viscosity  $\mu$ , it can be seen from [24] that high-pressure/low-viscosity conditions improve the seal stability.

It should be noted that  $K_s^*$  and  $D_s^*$  in Eq. [24] may include elastomeric stiffness and damping components which are frequency dependent. In such cases, an iterative process is required in solving Eq. [24] for  $\omega_{cr}$ .

It is of interest to obtain the precession  $\dot{\psi}$  of the stator at the stability threshold. The general form of the exponent  $\lambda$  in Eq. [16a] is  $\lambda = a + i\dot{\psi}$  but at the stability threshold  $a = 0$  and hence,

$$\lambda = i\dot{\psi}$$

Substituting in Eq. [18] and equating separately real and imaginary parts to zero gives, respectively

$$I^2\dot{\psi}^4 - (2IK + D^2)\dot{\psi}^2 + (K^2 + B^2) = 0$$

and

$$I\dot{\psi}^2 = K$$

from which it can be easily found that

$$\dot{\psi}_s = \frac{B}{D} = \frac{1/2}{1 + D/D_f} \quad [25]$$

where the index *s* indicates stability threshold.

### STEADY-STATE RESPONSE

Due to their linear nature, the angular equations of motion [66] and [67] can be solved separately for the effects of the forcing functions caused by  $\gamma_r$  and  $\gamma_o$ , respectively. The solution of these equations will be presented for each one of the two forcing functions in the most appropriate reference system. Hence, for the forcing function resulting from the rotor runout vector  $\gamma_r$ , which is rotating at the shaft speed, the solution will be performed in the rotating reference  $x'y_z$ . For the forcing function resulting from the initial misalignment of the stator  $\gamma_o$ , which is fixed in space, the solution will be performed in the inertial reference  $XYZ$ .

Starting with the effect of rotor runout alone requires  $M_{\gamma_o} = 0$ . Also, at steady state and in the absence of  $\gamma_o$ , the stator precesses at a constant rate  $\dot{\psi}$ . Its tilt vector  $\gamma_o$ , caused by the rotating vector  $\gamma_r$ , has a fixed value  $\gamma_r = \gamma_o$  and is rotating at the same speed as  $\gamma_r$ . The resultant relative misalignment vector  $\gamma$  (see Fig. 6) has, therefore, a constant value too, and is rotating at the same speed as  $\gamma_r$  and  $\gamma_o$ , namely, at the shaft speed. Hence,  $\dot{\psi} = \dot{\phi}_1 = 1$  where  $\dot{\psi}$  and  $\dot{\phi}_1$  are dimensionless parameters normalized by  $\omega$ . Using Eqs. [8a], [8b], [9a], [9b], and [61], and substituting  $\gamma_r = \gamma_o = \text{constant}$ , as well as  $\dot{\gamma} = \dot{\psi} = 0$ , we have

$$\begin{aligned} I\gamma_o &= -K\gamma_o - K_f\gamma\cos\phi' + \frac{1}{2}D_f\gamma\sin\phi' + K\gamma\cos\phi' \\ 0 &= -D\gamma_o - K_f\gamma\sin\phi' - \frac{1}{2}D_f\gamma\cos\phi' - K\gamma\sin\phi' \end{aligned} \quad [26]$$

From Fig. 6, we see that

$$\begin{aligned} \gamma\cos\phi' &= \gamma_o - \gamma_o\cos\phi' \\ \gamma\sin\phi' &= \gamma_o\sin\phi' \end{aligned} \quad [27]$$

Substituting [27] in [26], using Eqs. [5a] and [5b] and rearranging, we have:

$$\begin{aligned} (K - I)\gamma_o &= \left(K\cos\phi' + \frac{1}{2}D_f\sin\phi'\right)\gamma_r \\ \left(D + \frac{1}{2}D_f\right)\gamma_o &= \left(-K\sin\phi' + \frac{1}{2}D_f\cos\phi'\right)\gamma_r \end{aligned} \quad [28]$$

Adding the squares of the right- and left-hand sides of Eq. [28], respectively, gives the transmissibility of the system in the form

$$\left(\frac{\gamma_o}{\gamma_r}\right)^2 = \frac{K^2 + \frac{1}{4}D_f^2}{(K - I)^2 + \left(D + \frac{1}{2}D_f\right)^2} \quad [29]$$

The steady-state response to an initial stator misalignment  $\gamma_o$  alone is obtained by substituting  $\gamma_r = 0$  in Eqs. [66] and [67]. Hence, using again the complex form [15], we have

$$I\dot{\gamma}_r + D\dot{\gamma}_r + K\gamma_r - i\frac{1}{2}D_f\gamma_r = K\gamma_o \quad [30]$$

Since  $\gamma_o$  is fixed in space and has a constant magnitude, the response  $\gamma_r = \gamma_d$  will also be fixed in space and will have a constant magnitude. Thus,  $\dot{\gamma}_r = \dot{\gamma}_d = 0$  and Eq. [30] yields

$$\gamma_d = \frac{K\gamma_o}{\left(K^2 + \frac{1}{4}D_f^2\right)^{1/2}} \quad [31a]$$

and

$$\tan\psi_d = \frac{D_f}{2K} \quad [31b]$$

where  $\psi_d$  is the shift angle of the vector  $\gamma_d$  with respect to the real axis *X* in the complex plane *XY*.

In Eqs. [29] and [31], the stiffness *K* contains the flexible support stiffness *K<sub>s</sub>* according to [5a]. When the support has an elastomeric secondary seal, its stiffness *K<sub>s</sub>* depends on the frequency of the forcing function. It is important, therefore, to distinguish between the *K<sub>s</sub>* values to be used in Eq. [29] where the forcing function frequency is  $\omega$ , and in Eq. [31] where the forcing function frequency is zero.

From Eqs. [29] and [31], the complete steady-state response of the stator can now be expressed in the form

$$\vec{\gamma}_s = \vec{\gamma}_o + \vec{\gamma}_d \quad [32]$$

Since  $\vec{\gamma}_d$  is fixed in space but  $\vec{\gamma}_o$  is rotating at the speed  $\omega$ , the resultant vector  $\vec{\gamma}_s$  will also rotate at the speed  $\omega$  and its magnitude will vary cyclically.

The relative misalignment between stator and rotor, which is the more important parameter for seal performance, is obtained from [1] and [32] in the form

$$\vec{\gamma} = \vec{\gamma}_o + \vec{\gamma}_d \quad [33]$$

where

$$\vec{\gamma}_o = \vec{\gamma}_s - \vec{\gamma}_r$$

is the relative misalignment in the case  $\gamma_r = 0$ . The vector  $\gamma_o$  has a fixed value and is rotating at the speed  $\omega$ . Figure 7



54. It can be differentiated with respect to  $\rho$  to give the maximum transmissibility

$$\left(\frac{\gamma_o}{\gamma_r}\right)_{\max} = \frac{1}{2\xi(1-\xi^2)^{1/2}} \quad [39]$$

at the frequency ratio

$$\rho = \frac{1}{(1-2\xi^2)^{1/2}} \quad [40]$$

From Eq. [40], it is clear that the transmissibility in Eq. [38] has a maximum only for  $\xi^2 < \frac{1}{2}$ , in which case by [39]  $(\gamma_o/\gamma_r)_{\max} > 1$ . For  $\xi^2 > \frac{1}{2}$ , the transmissibility in [38] does not reach an extremum and is always less than unity namely,  $\gamma_o < \gamma_r$  for any  $\rho$ . As  $\rho$  increases indefinitely, the transmissibility in [38] approaches unity for any  $\xi$ . For small values of  $\xi$ , the maximum transmissibility in [39] can reach very high values when the seal operates near its resonance  $\rho \rightarrow 1$ . From the above discussion, it can be concluded that the best choice of  $\xi$  for keeping  $\gamma_o$  minimum is  $1/\sqrt{2} < \xi < 1$ , where  $\xi = 1$  corresponds to critical damping which results in fastest decay of any disturbance.

The critical speed  $\omega_c$  of Eq. [24] can be expressed in terms of the natural frequency  $\omega_n$  giving

$$\omega_c = 2\omega_n \left(1 + \frac{D^*}{D_f^*}\right) \quad [41]$$

Thus, the critical speed is at least twice the natural frequency of the system and can be avoided altogether by designing the seal to operate below its natural frequency. This can be obtained by selecting optimum coning that maximizes the fluid film stiffness [see Ref. (7)].

As was shown above the rotor runout,  $\gamma$ , has a direct effect on the relative misalignment  $\gamma$  which can cause failure due to local face contact. Because of manufacturing tolerances, a certain runout is inevitable. Thus, an important question in noncontacting seal design is how much rotor runout can be allowed before face contact occurs. The analysis presented here was based on small perturbation from the position of parallel faces. Face contact represents a large deviation from this case and, hence, may be unsuitable for handling by the present theory. Yet, it is worthwhile to examine the conditions for face contact even by the results of the small perturbation analysis which provide general trends, and also because when a more elaborate analysis becomes available, the validity of the relatively simple present one can be evaluated.

Rewriting Eq. [2] in its dimensionless form, noting that for small perturbation any axial disturbance of the stator dies out after a while, thus, at steady state  $Z = 0$ ,  $C = C_m$ , we have

$$H = 1 + \gamma R \cos \theta + \beta(R - R_i) \quad [42]$$

Face contact will first occur at  $\theta = \pi$  either at the inside or outside radius of the seal depending on the amount of coning  $\beta$ . The conditions for face contact are then from [42]

$$1 - \gamma R_i = 0 \quad [43a]$$

for contact at  $R = R_i$  and

$$1 - \gamma + \beta(1 - R_i) = 0 \quad [43b]$$

for contact at  $R = 1$ .

Solving Eqs. [43] for  $\gamma$  gives two different values, the smaller of which determines the appropriate contact condition. From Eqs. [43], it can be seen that the solution for  $\gamma$  is identical in the case  $\beta = 1/R_i$ . For  $\beta < 1/R_i$ , contact occurs at the outside radius  $R = 1$ , while for  $\beta > 1/R_i$ , contact occurs at the inside radius  $R = R_i$ . From the discussion following Eq. [20], it is clear that for the case  $P_o > P_i$ , the optimum coning  $\beta_{opt} = 2/R_i(1 - R_i)$  is larger than the critical one  $\beta_c = 1/R_i$ . Hence, for any reasonable seal design, face contact may occur according to condition [43a] when  $\gamma = 1/R_i$ . From Eq. [34], it is clear that  $\gamma$  reaches its maximum value at  $\tau = 0$ , in which case  $\gamma = \gamma_o + \gamma_d$ . Hence, for  $\beta > \beta_c$ , face contact occurs when

$$\gamma_o + \gamma_d = \frac{1}{R_i} \quad [44]$$

The relative tilt  $\gamma_o$  is related to the rotor runout by the relative transmissibility  $T = \gamma_o/\gamma_r$  given by Eq. [37]. Thus, Eq. [44] can be written in the form

$$T(\gamma_r)_{cr} + \gamma_d = \frac{1}{R_i}$$

Hence, the critical rotor runout causing face contact is

$$(\gamma_r)_{cr} = \frac{\frac{1}{R_i} - \gamma_d}{T} \quad [45]$$

where  $\gamma_d$  is given by Eq. [31a] and  $T$  by the square root of Eq. [37]. To avoid face contact, the critical rotor runout  $(\gamma_r)_{cr}$  should be as large as possible. From [45], it is clear that this will be achieved by reducing  $\gamma_d$  and  $T$ . Hence, the same factors that reduce the relative misalignment  $\gamma$  increase the critical rotor runout.

In conclusion of the discussion, a numerical example will now be presented to demonstrate the validity of the small perturbation assumption in practical cases. A typical seal with the following design parameters and operating conditions was selected as follows:

Seal outer radius, $r_o$ .....	0.04 m
Radius ratio, $R_i$ .....	0.8
Design clearance, $C_m$ .....	$10^{-5}$ m
Face taper (cone height) .....	$2.5 \times 10^{-5}$ m
S rotor mass, $m^*$ .....	1 kg
Shaft speed, $\omega$ .....	$10^3$ rad/s
Pressure differential, $p_o - p_i$ .....	$5 \times 10^5$ Pa
Fluid viscosity, $\mu$ (water at 60°C) .....	0.5 mPa s
Support stiffness, $K^*$ .....	$5 \times 10^5$ N/m
Support damping, $D^*$ .....	300 N s/m



The support stiffness and damping coefficients correspond to a Buna N secondary seal O-ring at the given shaft frequency. The corresponding dimensionless parameters for this example are

Coning angle, $\beta$ .....	12.5
Mass, $m$ .....	$3.25 \times 10^{-3}$
Inertia, $I$ .....	$1.63 \times 10^{-3}$
Pressure differential, $P_o - P_i$ .....	0.26
Support axial stiffness, $K_{33}$ .....	$1.63 \times 10^{-3}$
Support angular stiffness, $K_t$ .....	$8.14 \times 10^{-4}$
Support axial damping, $D_{33}$ .....	$9.76 \times 10^{-4}$
Support angular damping, $D_t$ .....	$4.88 \times 10^{-4}$
Fluid film angular stiffness, $K_f$ .....	$0.118 \times 10^{-1}$
Fluid film angular damping, $D_f$ .....	$0.83 \times 10^{-2}$

For this example, the calculated critical speed is  $\omega_c = 5.9\omega$ . The ratio  $\gamma_r/\gamma_s = 0.06$ , and the relative transmissibility is  $\gamma_r/\gamma_s = 0.14$ . Hence, for a rotor runout of  $10 \mu\text{m}$  at the outer diameter of the seal, which is a fairly large runout corresponding to  $\gamma_r = 1$ , and for an initial tilt of the stator of the same order of magnitude, the maximum relative misalignment  $\gamma$  is only about 0.20. It should be noted that, in the present example, several parameters were selected with the intention to make the transmissibility of order 0.1. In many practical cases, the design clearance and shaft speed will be smaller and the fluid viscosity, pressure differential, support and fluid film stiffness and damping will be larger. In these cases, the relative transmissibility will be even less than 0.1 and the assumption of small perturbation more realistic. From the above example, it can be seen that the critical speed  $\omega_c$  is very high. Hence, seal stability should not be a problem in conventional applications. The small perturbation analysis predicts the stability threshold quite accurately as can be seen from Eqs. [23a] and [23b]. Hence, Eq. [24] for  $\omega_c$  is valid without restrictions and can be used to examine stable operation of any noncontacting seal.

## CONCLUDING REMARKS

The dynamic behavior of a noncontacting face seal was analyzed taking into account manufacturing and assembly tolerances in the form of rotor runout and stator misalignment. Complete fluid film as well as flexible support dynamic effects were included. The equations of motion in the three major degrees of freedom of the seal were presented and solved analytically. The solution provides a stability threshold in terms of a critical speed below which stable seal operation is assured. Steady-state response to rotor runout in the presence of stator initial misalignment was found and expressed in terms of relative transmissibility. This enables calculation of the relative misalignment between stator and rotor as affected by the manufacturing and assembly tolerances, by the design parameters, and by the seal operation conditions. It was shown that, in the presence of both rotor runout and stator initial misalignment, the relative misalignment is time dependent and varies cyclically at shaft rotation frequency. A critical rotor runout was found related to various design parameters and operating conditions. This critical value can give the designer and manufacturer an idea of the magnitude of rotor runout

which can still be tolerated without causing failure by face contact.

A numerical example was presented to demonstrate the validity of the small perturbation assumption in practical applications. It was also shown that stability threshold usually does not present a problem and its prediction by the small perturbation analysis is comparable with this of a more elaborate numerical one.

It is hoped that the information provided here will direct the attention of seals designers and users to the various factors affecting noncontacting seals performance, and that, based on this information, careful experimentation will be carried out to evaluate the theoretical results.

## ACKNOWLEDGMENT

The research reported here was supported in parts by the Israel Academy of Sciences and the US Air Force Wright Aeronautical Labs/AFWAL/POSL under contract F49620-83-C-0057.

## REFERENCES

- (1) Etsion, I., "A Review of Mechanical Face Seal Dynamics," *Shock and Vibration Digest*, **14**, 3, pp 9-14 (1982).
- (2) DiRusso, E., "Film Thickness Measurements for Spiral Groove and Rayleigh Step Lift Pad Self-Acting Face Seals," NASA TP-2058, Oct 1982.
- (3) Schnal, J., Sedv, J., Zobens, A., and Etsion, I., "Performance of the Coned-Face End Seal with Regard to Energy Conservation," *ASLE Trans.*, **26**, 4, pp 415-429 (1983).
- (4) Etsion, I. and Constantinescu, I., "Experimental Observation of the Dynamic Behavior of Non-Contacting Coned-Face Mechanical Seals," *ASLE Trans.*, **27**, 3, pp 263-270 (1984).
- (5) Metcalfe, R., "Dynamic Tracking of Angular Misalignment in Liquid Lubricated End-Face Seals," *ASLE Trans.*, **24**, 4, pp 509-516 (1981).
- (6) Etsion, I., "Dynamic Analysis of Noncontacting Face Seals," *Trans. ASME J. Lubr. Tech.*, **104**, 4, pp 460-468 (1982).
- (7) Green, I. and Etsion, I., "Fluid Film Dynamic Coefficients in Mechanical Face Seals," *Trans. ASME J. Lubr. Tech.*, **105**, 2, pp 297-302 (1983).
- (8) Green, I. and Etsion, I., "Stiffness and Damping Characteristics of Elastomer O-Rings Secondary Seals Subjected to Reciprocating Twist," *Proc. 10th Intl. Conf. Fluid Sealing*, BHRA, April 1984, pp 221-229.
- (9) Thomson, T. W. *Theory of Vibration with Applications*, Prentice-Hall, 2nd Ed. (1981).
- (10) Green, I. and Etsion, I., "A Kinematic Model for Mechanical Seals with Antirotation Locks or Positive Drive Devices," Report EEC-153, Dept. of Mech. Eng., Technion, Haifa, Israel, June 1984.

## APPENDIX 1

### Angular Stiffness and Damping Coefficients of the Flexible Support

Usually the axial stiffness and damping coefficients of the flexible support are measurable and known. The angular coefficients can be obtained from the axial ones. Figure 8 shows a model of the seal in which the stator has a displacement  $Z$  and a tilt  $\gamma$ , about axis  $x$ . The axial displacement of a point  $B$  located at a radius  $r$ , is

$$Z_B = Z + r\gamma\cos\theta \quad [46]$$

where  $r$ , is a general radial location of the flexible support, and  $\theta$  is given by

$$\theta = \phi - \psi \quad [47]$$

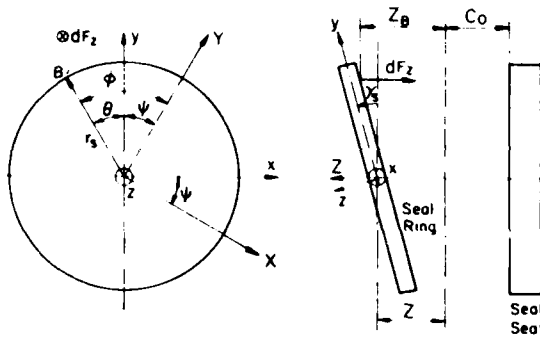


Fig. 8—A model for calculating angular stiffness and damping coefficients of the secondary seal.

The axial velocity of point  $B$  is therefore

$$\dot{Z}_B = \dot{Z} + r_s \dot{\gamma} \cos \theta + r_s \dot{\psi} \sin \theta \quad [48]$$

Due to the motion of point  $B$  an axial force  $dF_z$  is generated, its value is

$$dF_z = -Z_B dK_{33} - \dot{Z}_B dD_{33} \quad [49]$$

where  $dK_{33}$  and  $dD_{33}$  are infinitesimal stiffness and damping coefficients, respectively. Assuming uniform circumferential distribution of the dynamic properties of the flexible support, we have

$$dK_{33} = \frac{K_{33} d\theta}{2\pi} \quad [50]$$

$$dD_{33} = \frac{D_{33} d\theta}{2\pi} \quad [51]$$

The moments acting on the stator due to the flexible support are then:

about the  $x$  axis

$$M_1 = \int_0^{2\pi} r_s \cos \theta dF_z \quad [52]$$

and about the  $y$  axis

$$M_2 = \int_0^{2\pi} r_s \sin \theta dF_z \quad [53]$$

Substituting Eqs. [46], and [48] through [51] and integrating [52] and [53] gives

$$M_1 = -\frac{1}{2} (K_{33} r_s^2 \dot{\gamma}_x + D_{33} r_s^2 \dot{\gamma}_x) \quad [54]$$

$$M_2 = -\frac{1}{2} D_{33} r_s^2 \dot{\gamma}_y \psi \quad [55]$$

By definition, we find

$$K_{11} = -\frac{\partial M_1}{\partial \gamma} = \frac{K_{33}}{2} r_s^2 \quad [56]$$

$$D_{11} = -\frac{\partial M_1}{\partial \dot{\gamma}} = \frac{D_{33}}{2} r_s^2 \quad [57]$$

$$K_{12} = -\frac{\partial M_2}{\partial \gamma} = \frac{D_{33}}{2} r_s^2 \dot{\psi} = D_{11} \dot{\psi} \quad [58]$$

## APPENDIX 2

### The Equations of Motion

In Ref. (10), a kinematic model of a mechanical seal was presented and the dynamic moments for the case of a flexibly mounted stator with antirotation locks were obtained in the form:

$$T_x = I(\ddot{\gamma}_x - \dot{\psi}^2 \gamma_x) \quad [59]$$

$$T_y = I(\ddot{\psi} \gamma_y + 2\dot{\psi} \dot{\gamma}_y)$$

It was also shown in (10) that the moment  $T_z$  is of order  $\dot{\gamma}^2$  and, hence, can be neglected.

The dynamic moments in the inertial system  $XYZ$  are simply

$$T_x = I\ddot{\gamma}_x \quad [60]$$

$$T_y = I\ddot{\gamma}_y$$

where  $\gamma_x$  and  $\gamma_y$  are the components of  $\gamma$ , along the inertial axes  $X$  and  $Y$ , respectively.

The angular equations of motion can now be obtained in the rotating system  $xyz$  or in the inertial system  $XYZ$  by simply equating the dynamic moments  $\vec{T}$  with their corresponding applied moments  $M$ . Hence, with the aid of Fig. 6, the equations of motion in the  $xyz$  system for the angular degrees of freedom are

$$I(\ddot{\gamma}_x - \dot{\psi}^2 \gamma_x) = M_x + M_{f1} \cos \phi - M_{f2} \sin \phi + M_{x\phi} \cos \psi + M_{y\phi} \cos \phi' \quad [61]$$

$$I(\ddot{\psi} \gamma_y + 2\dot{\psi} \dot{\gamma}_y) = M_y + M_{f1} \sin \phi + M_{f2} \cos \phi - M_{x\phi} \sin \psi - M_{y\phi} \sin \phi'$$

In the inertial  $XYZ$  system, these equations are

$$I\ddot{\gamma}_x = M_{x\phi} + M_{f1} \cos \phi_1 - M_{f2} \sin \phi_1 + M_{x\phi} + M_{y\phi} \cos \omega t \quad [62]$$

$$I\ddot{\gamma}_y = M_{y\phi} + M_{f1} \sin \phi_1 + M_{f2} \cos \phi_1 + M_{y\phi} \sin \omega t$$

where  $M_{x\phi}$  and  $M_{y\phi}$ , which are the flexible support induced moments during operation, replace the moments  $M_x$  and  $M_y$ . These new introduced moments are simply

$$\begin{aligned} M_{1X} &= -K_{11}\gamma_X - D_{11}\dot{\gamma}_X \\ M_{1Y} &= -K_{11}\gamma_Y - D_{11}\dot{\gamma}_Y \end{aligned} \quad [63]$$

The fluid film induced moments  $M_{f1}$  and  $M_{f2}$  are given in Eqs. [9a] and [9b] in terms of the relative misalignment  $\gamma$ . It will be useful to express them in Eq. [62] in terms of the angles  $\gamma_X$  and  $\gamma_Y$ . From Fig. 4, we can see that

$$\begin{aligned} \gamma_X &= \gamma \cos \phi_1 + \gamma_r \cos \omega t \\ \gamma_Y &= \gamma \sin \phi_1 + \gamma_r \sin \omega t \end{aligned} \quad [64]$$

Differentiating with respect to time, we have

$$\begin{aligned} \dot{\gamma} \cos \phi_1 - \gamma \dot{\phi}_1 \sin \phi_1 &= \dot{\gamma}_X + \gamma_r \sin \omega t \\ \dot{\gamma} \sin \phi_1 + \gamma \dot{\phi}_1 \cos \phi_1 &= \dot{\gamma}_Y - \gamma_r \cos \omega t \end{aligned} \quad [65]$$

Hence, by [5a], [5b], [9a], [9b], [62], and [65] Eqs. [62] can be rearranged in the form

$$I\ddot{\gamma}_X + D_{11}\dot{\gamma}_X + K_{11}\gamma_X + \frac{1}{2}D_{f11}\gamma_Y = \gamma_r \left( K_{11} \cos \omega t - \frac{1}{2}D_{f11} \sin \omega t \right) + K_{11}\gamma_a \quad [66]$$

$$\begin{aligned} I\ddot{\gamma}_Y + D_{11}\dot{\gamma}_Y + K_{11}\gamma_Y - \frac{1}{2}D_{f11}\gamma_X \\ = \gamma_r \left( K_{11} \sin \omega t + \frac{1}{2}D_{f11} \cos \omega t \right) \end{aligned} \quad [67]$$

Equations [66] and [67] are coupled but are linear. It can also be seen that the rotor runout  $\gamma_r$  and the initial misalignment of the stator  $\gamma_a$  form forcing functions of the dynamic system.

The equation of motion in the axial degree of freedom is simply

$$m\ddot{Z} = F_Z \quad [68]$$

APPENDIX D  
NONLINEAR DYNAMIC ANALYSIS OF NONCONTACTING  
CONED-FACE MECHANICAL SEALS



# Nonlinear Dynamic Analysis of Noncontacting Coned-Face Mechanical Seals<sup>©</sup>

I. GREEN and I. ETSION (Member, ASLE)  
Technion, Haifa 32000, Israel

*The complete nonlinear equations of motion of a flexibly mounted stator in a noncontacting coned-face mechanical seal are solved numerically. The solution utilizes a transient dynamic analysis and takes into account rotor axial runout and assembly tolerances in the form of initial stator misalignment. Cavitation of the fluid film is also accounted for. A parametric investigation is performed and the effect of various design parameters and operation conditions on the seal dynamics is presented and discussed. A critical shaft speed is found above which the seal becomes dynamically unstable. A critical rotor runout is found which, if exceeded, will cause seal failure due to local face rubbing contact. A comparison is made*

*between the numerical results and those of a simpler analytical solution. It is found that the analytical solution is valid for most practical applications of mechanical seals.*

## INTRODUCTION

In a previous paper (1), a dynamic analysis based on small perturbation was performed for a noncontacting coned-face mechanical seal. The analysis took into account rotor axial runout and assembly tolerances in the form of initial stator misalignment. Both stability threshold and steady-state response of the seal system were investigated. A critical speed was found above which the seal becomes unstable. In the stable mode of operation, the flexibly mounted stator tracks the rotor with a certain relative misalignment which depends, among other factors, on the amount of rotor runout and assembly tolerances. For large runouts, this relative misalignment can become dangerously high and cause seal

Presented at the 40th Annual Meeting  
in Las Vegas, Nevada  
May 6-9, 1985  
Final manuscript approved January 22, 1985

## NOMENCLATURE

$C$  = centerline clearance  
 $C_d$  = design clearance  
 $D^*$  = damping coefficient  
 $D$  = dimensionless damping  
 $F_z$  = dimensionless axial force  
 $H$  = dimensionless film thickness,  $h/C_d$   
 $H_c$  = face taper  
 $h$  = local film thickness  
 $I$  = dimensionless moment of inertia  
 $K^*$  = stiffness coefficient  
 $K$  = dimensionless stiffness  
 $M$  = dimensionless moment  
 $m$  = dimensionless mass  
 $P$  = dimensionless pressure,  $p/S$   
 $p$  = pressure  
 $R$  = dimensionless radial coordinate,  $r/r_o$   
 $r$  = radial coordinate  
 $S$  = seal parameter,  $6\mu\omega(r_o/C_d)^2 (1-R_c)^2$   
 $t$  = time  
 $Z^*$  = axial displacement  
 $Z$  = dimensionless displacement  $Z^*/C_d$

$\beta^*$  = face coning  
 $\beta$  = dimensionless coning,  $\beta^*r_o/C_d$   
 $\gamma^*$  = relative misalignment  
 $\gamma$  = dimensionless misalignment,  $\gamma^*r_o/C_d$   
 $\gamma_o$  = dimensionless relative misalignment caused by rotor runout alone  
 $\gamma_r$  = dimensionless rotor runout  
 $\gamma_n$  = dimensionless tilt of stator (nutation)  
 $\gamma_{oi}$  = stator dimensionless initial misalignment  
 $\gamma_{oi}$  = stator response due to  $\gamma_{oi}$  alone  
 $\gamma_{ro}$  = stator response due to  $\gamma_r$  alone  
 $\theta$  = angular coordinate  
 $\mu$  = viscosity  
 $\psi$  = precession  
 $\omega$  = shaft angular velocity

## Subscripts

$cr$  = critical  
 $f$  = fluid film  
 $i$  = inner radius  
 $m$  = mid radius  
 $o$  = outer radius  
 $s$  = stator, or flexible support

failure due to excessive leakage or local face contact. A critical runout was found in (1) which, if exceeded, will result in local face contact.

The assumption of small perturbation from the position of parallel faces, on which the analysis in (1) is based, leads to a linearization of the equations of motion of the seal ring. This enables closed-form analytical solution and yields very useful analytical expressions for seal dynamic performance. However, the small perturbation assumption may be restrictive in cases where the faces are far from being parallel. The case of critical rotor runout, for example, may be inappropriate for handling by the small perturbation analysis since it corresponds to high relative misalignment between the seal faces. Another restriction of the small perturbation assumption is the neglect of cavitation and nonlinear effects on the dynamic properties of the fluid film. Hence, high-speed low-pressure cases may be ill treated by the simple analysis. In order to cover the full range of seal operation conditions, and to obtain a complete picture of its dynamic behavior, the small perturbation restriction has to be relaxed, and all the nonlinear effects have to be accounted for. This requires a numerical transient solution of the complete dynamic equations of the seal. It is the purpose of this report to present the results of such an effort. In addition, a comparison will be made with the results obtained by the small perturbation analysis of Ref. (1). This will determine the range of validity of the simpler and more convenient to use analysis of (1).

## BACKGROUND AND METHOD OF SOLUTION

The seal model is shown in Fig. 1. It consists of a seal seat (rotor) that is rigidly mounted to the rotating rigid shaft, and a flexibly supported seal ring (stator). The rotor has an axial runout that can be represented by a tilt  $\gamma^*$  of its plane with respect to the axis of shaft rotation. Similarly, the stator may have, prior to final attachment to the rotor [see (1)], an initial misalignment  $\gamma_a^*$  with respect to the axis of shaft rotation. At rest, and with zero pressure differential, the stator is pressed against the rotor by the supporting springs alone. This forces the stator into the same tilt,  $\gamma^*$ , as that of the rotor. During operation, the mating faces separate and the stator assumes a new tilt  $\gamma^*$ . This tilt is a result of the combined effects of both  $\gamma^*$  and  $\gamma_a^*$ . The tilt angles  $\gamma_a^*$ ,  $\gamma^*$ , and  $\gamma$  are all very small, of the order of

a few milliradians, and, hence, can be treated as vectors. Since  $\gamma_a^*$  is fixed in space and  $\gamma^*$  is rotating at the shaft speed  $\omega$ , the resultant vector  $\gamma^*$  will possess a time-varying speed,  $\psi$ . In Ref. (1), it was found that the vector  $\gamma^*$  can be expressed in the dimensionless form (see Nomenclature for  $\gamma^*$  and  $\gamma$ ):

$$\vec{\gamma} = \vec{\gamma}_a + \vec{\gamma}_r \quad [1]$$

where  $\vec{\gamma}_a$  is fixed and is the response to  $\vec{\gamma}_a$  alone, and  $\vec{\gamma}_r$  is rotating and is the response to  $\vec{\gamma}_r$  alone. As will be shown later, a similar presentation of  $\vec{\gamma}$ , is possible in the nonlinear case, too. The relative misalignment,  $\gamma$ , between the stator and rotor is also a rotating vector given by the vector subtraction

$$\vec{\gamma} = \vec{\gamma}_r - \vec{\gamma}_a \quad [2]$$

Figure 2 shows the relative position between the seal components and Fig. 3 gives a vector representation of the various tilts of the seal system. The vector  $\gamma_a$  in Fig. 3 is the relative misalignment  $\gamma$  in the special case  $\gamma_a = 0$  and is simply:

$$\vec{\gamma}_r = \vec{\gamma}_r - \vec{\gamma}_a \quad [3]$$

The equations of motion of the flexibly mounted stator are [see Ref. (1)]:

$$I(\ddot{\gamma}_x - \dot{\psi}^2 \gamma_x) = M_x \quad [4]$$

$$I(\ddot{\gamma}_y + 2\dot{\psi}\dot{\gamma}_y) = M_y \quad [5]$$

$$m\ddot{Z} = F_z \quad [6]$$

where  $M_x$  and  $M_y$  are the moments acting on the stator about axes  $x$  and  $y$ , respectively, of a reference system  $xyz$  which rotates at a rate  $\dot{\psi}$  in an inertial system  $XYZ$  [see Figs. 2(a) and 3]. The axis  $x$  of the rotating system coincides with the vector  $\vec{\gamma}$ , and is at an angle  $\psi$  with respect to the inertial axis  $X$ .

The moments  $M_x$  and  $M_y$  as well as the axial force  $F_z$  consist of contributions from both the flexible support and the fluid film. The support contribution to the moments and forces is (1):

$$M_x = K[\gamma_a \cos \psi + \gamma_r \cos(\psi - \omega t) - \gamma_r] - D\dot{\gamma}_x \quad [7]$$

$$M_y = -K[\gamma_a \sin \psi + \gamma_r \sin(\psi - \omega t)] - D\dot{\gamma}_y \quad [8]$$

$$F_z = -K'Z - D'\dot{Z} \quad [9]$$

where  $K'$  and  $D'$  are axial stiffness and damping coefficients, respectively, of the support. These coefficients include the dynamic properties of the supporting springs and the secondary seal which can be a metal or elastomer bellows or elastomer ring. The dynamic properties of an elastomer

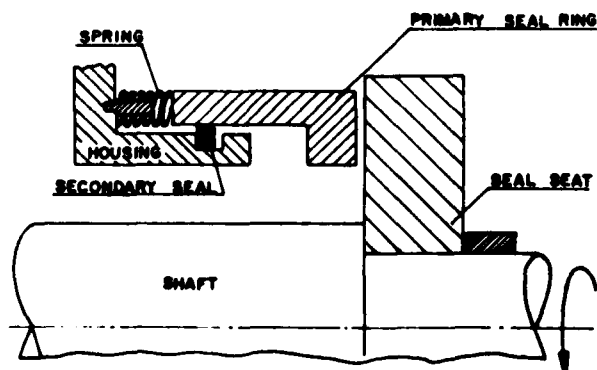


Fig. 1—Schematic of a radial face seal

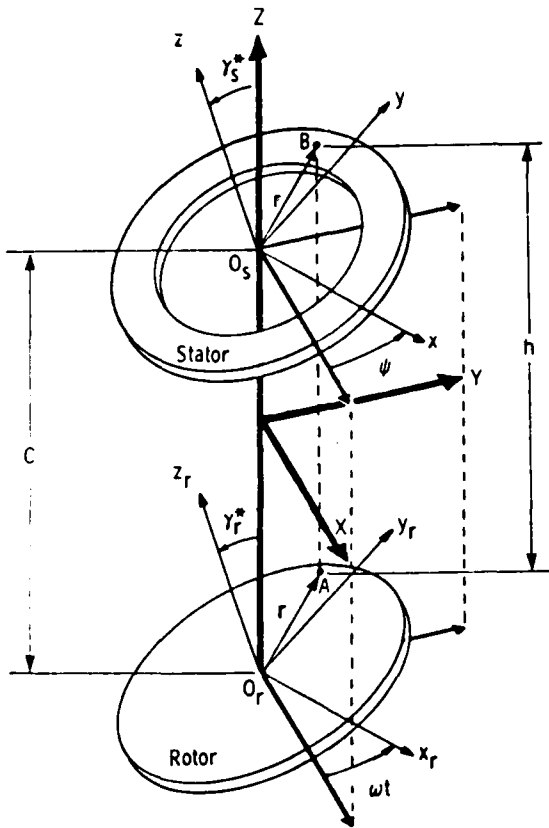


Fig. 2(a)—Seal model and coordinate systems

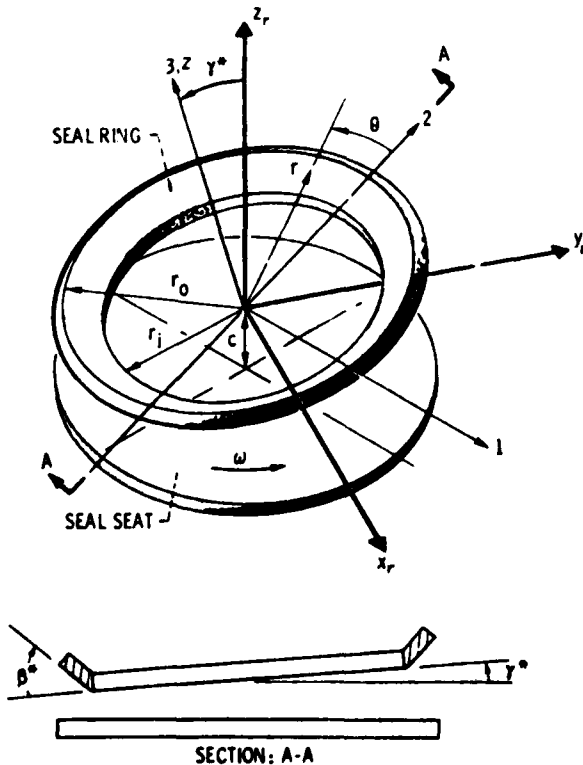


Fig. 2(b)—Relative position between seal ring and seal seat

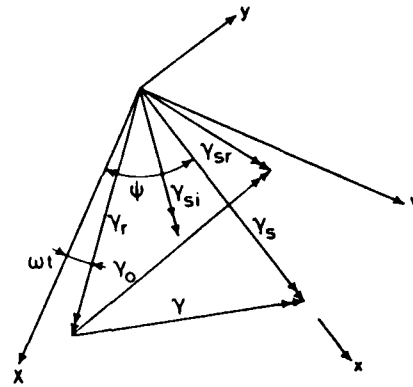


Fig. 3—Vector representation of tilts of the seal components

secondary seal can be obtained experimentally, e.g. (2). From the known coefficients  $K'_i$  and  $D'_i$ , one can calculate the angular stiffness and damping coefficients  $K_i$  and  $D_i$  (1). The terms  $\gamma_i$  and  $\gamma_{oi}$  in Eqs. [7] and [8] are due to the assembly tolerances ( $\gamma_{oi}$  is arbitrarily assumed to coincide with the negative  $X$  direction).

The fluid film contribution to  $M_x$ ,  $M_y$ , and  $F_z$  is obtained by first calculating the pressure distribution in the sealing gap and then integrating numerically over the face area. Expressions for the various fluid film pressure components were given elsewhere, e.g. (3), and are not repeated here. It should be noted, however, that cavitation is accounted for in the present analysis by deleting any negative pressure before integration. In addition, curvature effect due to the change in  $r$  is also accounted for in the numerical integration.

The dimensionless local film thickness is given by

$$H = 1 + \epsilon R \cos \theta + \delta (R - R_i) \quad [10]$$

where

$$\epsilon = \frac{\gamma}{1+Z}$$

and

$$\delta = \frac{\beta}{1+Z}$$

Since  $\gamma$  and  $Z$  are time dependent,  $H$  is time dependent, too.

The relationship between the various tilt angles is (see Fig. 3)

$$\gamma = [\gamma_r^2 + \gamma_s^2 - 2\gamma_r\gamma_s\cos(\psi - \omega t)]^{1/2} \quad [11]$$

Hence, starting with some arbitrary values for the initial conditions  $\gamma_i$ ,  $\psi$ ,  $Z$  and their corresponding time derivatives, the film thickness  $H$  can be calculated by Eqs. [10] and [11]. Next, the pressure field and the resulting moments  $M_x$ ,  $M_y$  and the force  $F_z$  are calculated. The time second derivatives

of the stator degrees of freedom:  $\dot{\gamma}$ ,  $\dot{\psi}$ , and  $\dot{Z}$  are then found from Eqs. [4] to [6] in the form:

$$\dot{\gamma} = \frac{M_\gamma}{I} + \dot{\psi}^2 \gamma, \quad [12]$$

$$\dot{\psi} = \left( \frac{M_\psi}{I} - 2\dot{\gamma} \right) / \gamma, \quad [13]$$

$$\dot{Z} = \frac{F_Z}{m} \quad [14]$$

These values are integrated with respect to time and new values are found for  $\dot{\gamma}$ ,  $\gamma$ ,  $\dot{\psi}$ ,  $\psi$ ,  $\dot{Z}$ , and  $Z$ . The minimum film thickness is checked at each time step and the procedure repeats itself until local face contact occurs, or until the minimum film thickness shows steady-state behavior over a few successive shaft revolutions. The computer program used is basically similar to that described in (4) with a few modifications. The time integration mentioned above was performed by the MILNE integration method of the CSMP (5) on an IBM 370/168 computer. The average computer time required was about 1 s per each revolution of the rotor, and it took at least six revolutions to determine the stability status of the seal system for a given set of operation conditions and design parameters.

## RESULTS AND DISCUSSION

The computer program enables one to describe the complete dynamic behavior of the seal. This includes both stator tracking of rotor runout in the stable mode of operation and dynamic stability threshold of the seal. As was shown in (1), the axial runout  $\gamma$ , and the initial misalignment of the stator,  $\gamma_0$ , form forcing functions and, hence, affect only the dynamic response at stable operation but not the dynamic stability. Yet, it is interesting to compare the stability threshold obtained from the numerical analysis with that obtained from the approximate analytical solution of Ref. (1).

A critical speed  $\omega_c$  was found in Ref. (1) above which the seal becomes unstable (stability threshold). The analytical expression for  $\omega_c$  in (1) is

$$\omega_c^2 = \frac{4K^*}{I^*} \left( 1 + \frac{K_f^*}{K^*} \right) \left( 1 + \frac{D_f^*}{D^*} \right)^2 \quad [15]$$

In Eq. [15]  $K^*$  and  $D^*$  are the angular stiffness and damping coefficients, respectively, of the support related to the axial coefficients,  $K_f^*$  and  $D_f^*$  by [see (1)]:

$$K^* = K_f^* \frac{r_s^2}{2}$$

and

$$D^* = D_f^* \frac{r_s^2}{2}$$

where  $r_s$  is the radial location of the flexible supporting

element. The expression for  $K_f^*$  and  $D_f^*$  are (6):

$$K_f^* = \pi(p_o - p_i) \frac{r_o^4}{C_o} (\beta R_i - 1) E_o^2$$

$$D_f^* = 12\pi\mu \frac{r_o^6}{C_o^3} (1 - R_i)^2 R_m^3 G_o$$

where

$$E_o = \frac{1 - R_i^2}{4 + 2\beta(1 - R_i)}$$

and

$$G_o = \frac{\ell n[1 + \beta(1 - R_i)] - 2 \frac{\beta(1 - R_i)}{2 + \beta(1 - R_i)}}{\beta^3(1 - R_i)^2}$$

The precession,  $\dot{\psi}_c$ , of the stator at the stability threshold was found in (1) in the form

$$\dot{\psi}_c = \frac{0.5}{1 + \frac{D_f^*}{D^*}} \quad [16]$$

A stability threshold search was performed, using the present computer program for 60 different cases to evaluate the accuracy of the small perturbation analysis in predicting seal stability. The range of radius ratios covered was between  $R_i = 0.7$  to  $R_i = 0.98$ . At each radius ratio, several combinations of  $K_f^*/K^*$  and  $D_f^*/D^*$  values were tested. These combinations consisted of the values 0.2, 0.4, 0.6, and 0.8 for  $K_f^*/K^*$ , and the values 0, 0.2, and 0.4 for  $D_f^*/D^*$ . A relatively low pressure differential, having the dimensionless value  $P_o - P_i = 0.25$ , was selected to facilitate unstable operation. The face coning  $\beta$  at each radius ratio was the optimal one for maximum  $K_f^*$ , and is given by [see (6)]:

$$\beta_{opt} = \frac{2}{R_i(1 - R_i)} \quad [17]$$

The numerical analysis gave critical speed values that were always slightly less than those given by Eq. [15]. The differences ranged from 4 percent at  $R_i = 0.7$  to only 1 percent at  $R_i = 0.98$ . The results for  $\dot{\psi}_c$  were identical to those of Eq. [16]. Hence, it can be concluded that the small perturbation analysis of Ref. (1) predicts quite accurately the stability threshold of the seal and Eq. [15] can be used safely to calculate the critical speed.

The effect of rotor axial runout and stator initial misalignment on the dynamic behavior is fully expressed in the stable mode of seal operation. The computer program was used to calculate the minimum film thickness  $(h/C_o)_{min}$ , the relative misalignment  $\gamma_0$  (and, hence the transmissibility  $\gamma_0/\gamma$ ), and the axial displacement  $Z$  of the flexibly mounted stator. This was done for various values of rotor axial runout,  $\gamma_r$ , and for  $\gamma_0 = 0$ . A very important result of these



calculations is the critical rotor runout  $(\gamma_r)_c$ , which causes local face contact namely,  $(h/C_o)_{min} = 0$ . Knowledge of the critical rotor runout is very helpful in setting reasonable manufacturing tolerances and in avoiding seal failure. Finally, the effect of assembly misalignment,  $\gamma_m$ , on the dynamic behavior was also examined. This misalignment prevents tracking with uniform nutation and precession. Hence, the relative misalignment between stator and rotor as well as the axial clearance become time dependent and vary cyclically at the shaft frequency.

Altogether there are ten different parameters which affect the seal dynamics. These are: the seal outer and inner radii, stator mass, fluid viscosity, pressure differential across the seal, designed axial clearance, face coning, shaft speed, and stiffness and damping of the flexible support. A parametric investigation which takes into account variations in all these parameters would require an enormous computer time. Hence, to overcome this problem without losing too much information, a "single perturbation" method was utilized. By this method, a reference case is set up for the ten parameters. Each of the more important parameters is perturbed one at a time and then regains its reference value. Solutions are obtained for each single perturbation resulting in reasonable amount of information from a relatively small number of variations. Many cases were examined by the analysis of (1) prior to selecting the reference case. In most practical cases, the transmissibility was found to be  $\gamma_o/\gamma_r \ll 1$ . Hence, most practical cases comply with the definition of small perturbation for which the results of Ref. (1) should be valid. This was, indeed, verified by solving some of these cases numerically and comparing the results with those of Ref. (1). The correlation was always within a few percent.

In order to determine the range of validity of the small perturbation analysis of (1), cases which were clearly out of the range of small perturbation were singled out and selected for the reference seal. These cases are characterized by relatively large mass, large axial clearance, very high shaft speed, low pressure differential, and low fluid viscosity. The seal selected for the reference case of the parametric investigation is a medium size seal with 80 mm outer diameter, and a 0.8 radius ratio, sealing water at temperature of 60°C and pressure of 0.3 MPa. The stator mass is 1 kg and the

designed sealing gap is 8  $\mu\text{m}$ . The stiffness and damping of the support are typical for Buna N O-ring (2). An optimum coning with 20- $\mu\text{m}$  taper was selected. Table 1 presents the reference case and the perturbations in the more important parameters. The stiffness and damping of the flexible support were increased or decreased simultaneously. The high values correspond to Viton 75 O-ring while the low values represent a metal-bellows secondary seal.

The results for the case  $\gamma_m = 0$  are shown in Figs. 4 through 8. Parts (a), (b), and (c) of each figure present the minimum film thickness  $(h/C_o)_{min}$ , the relative misalignment  $\gamma_m$ , and the axial displacement  $Z$ , respectively, as functions of the rotor runout  $\gamma_r$ . A comparison is made between the present numerical solution and the analytical solution of Ref. (1). From the part (a) of each of the Figs. 4 through 8, the critical rotor runout  $(\gamma_r)_c$  can be obtained from the intersection of the curves with the line  $(h/C_o)_{min} = 0$ . It is quite difficult to obtain exactly this intersection from the numerical solution due to the very large computer time required in cases of large runouts. However, the intersection can be obtained from the available numerical results by extrapolation. It should also be noted that as the rotor runout approaches its critical value, the axial displacement  $Z$  becomes very large [see part (c) of the figures]. Hence, in many cases, the seal may fail because of an excessive leakage much before local face contact occurs. It is also more practical to set a limit for the permissible minimum film thickness at, say,  $(h/C_o) = 0.25$ , and define the critical rotor runout as the value of  $\gamma_r$  corresponding to that limit. This will prevent the possibility of local face contact and will provide a factor of safety and a more practical value for the critical rotor runout. There were no difficulties in obtaining numerical solutions for cases of  $(h/C_o)_{min} \geq 0.25$ .

Figure 4 presents the effect of the design clearance  $C_o$ . From Fig. 4(a), it can be seen that the critical rotor runout obtained from the numerical solution is always larger than that predicted analytically. This is true for all the other cases as well [see part (a) of Figs. 5–8]. Hence, the analytical prediction may serve as an upper limit for the critical runout which, if not exceeded, assures noncontacting operation. The analytical  $(\gamma_r)_c$  values predicted for design clearances  $C_o$  of 12  $\mu\text{m}$ , 8  $\mu\text{m}$ , and 4  $\mu\text{m}$  are: 1.745, 3.319, and 8.290, respectively [Fig. 4(a)]. The axial runout at the outer radius

TABLE 1: PARAMETER VALUES FOR THE SINGLE PERTURBATION SOLUTION SCHEME

PARAMETER	LOW VALUE	REFERENCE	HIGH VALUE
Outer radius, $r_o$ , m	—	0.040	—
Inner radius, $r_i$ , m	—	0.032	—
Mass, $m^*$ , kg	—	1	—
Viscosity, $\mu$ , mPa·s	—	0.5	—
Design clearance, $C_o$ , $\mu\text{m}$	4	8	12
Shaft speed, $\omega$ , rad/s	1000	2000	3000
Pressure differential, $p_o - p_i$ , Pa	$10^5$	$3 \times 10^5$	$10^6$
Support stiffness, $K^*$ , N/m	$10^5$	$5 \times 10^5$	$2 \times 10^6$
Support damping, $D^*$ , Ns/m	0	300	2000
Face taper, $H_r$ , $\mu\text{m}$	10	20	40

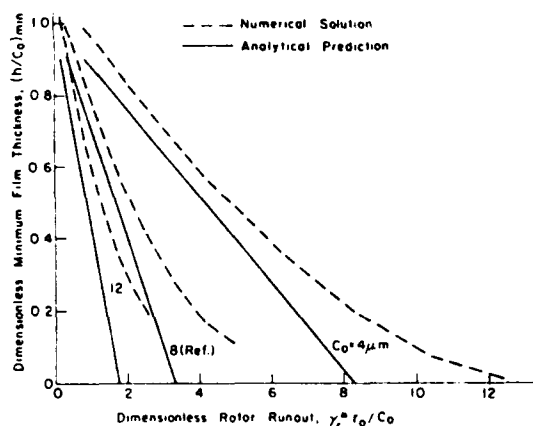


Fig. 4(a)—Minimum film thickness,  $(h/C_0)_{min}$ , vs rotor runout,  $\gamma_r$ , and designed clearance,  $C_0$ .

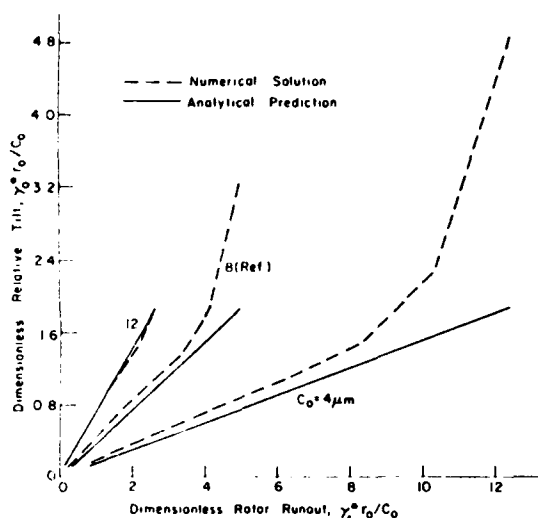


Fig. 4(b)—Relative tilt,  $\gamma$ , vs rotor runout,  $\gamma_r$ , and designed clearance,  $C_0$ .

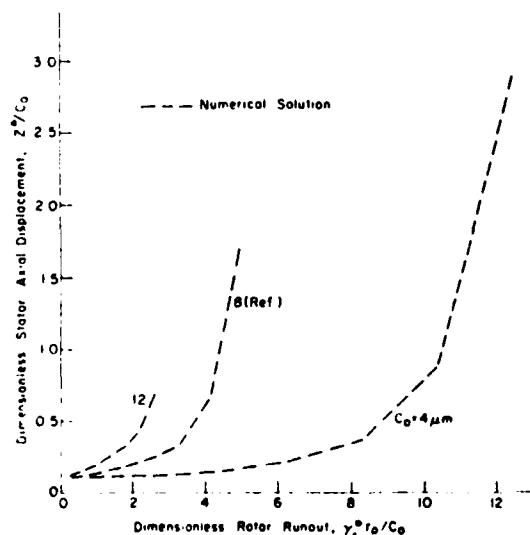


Fig. 4(c)—Axial displacement,  $Z$ , vs rotor runout,  $\gamma_r$ , and designed clearance,  $C_0$ .

$r_o$  due to rotor runout  $\gamma_r$  is:

$$r_o \gamma_r^* = C_0 \gamma_r$$

Hence, the corresponding values of critical axial runout for  $C_0$  values of 12  $\mu\text{m}$ , 8  $\mu\text{m}$ , and 4  $\mu\text{m}$  are: 21  $\mu\text{m}$ , 27  $\mu\text{m}$ , and 33  $\mu\text{m}$ , respectively. That means that the critical axial runout increases as the design clearance decreases. In other words, from the standpoint of preventing local face contact, it is better to design the seal with a small clearance. This is probably due to the fact that smaller  $C_0$  increases the fluid film stiffness and reduces the transmissibility  $\gamma_o/\gamma_r$ . From Fig. 4(a), we can also see that for smaller design clearance  $C_0$ , the analytical prediction becomes closer to the numerical solution. At  $(h/C_0)_{min} = 0.25$  for example, the analytical prediction requires runout values that are 19 percent, 29 percent, and 40 percent less than the corresponding numerical results for  $C_0$  values of 4  $\mu\text{m}$ , 8  $\mu\text{m}$ , and 12  $\mu\text{m}$ , respectively. Figure 4(b) shows the effect of  $C_0$  on the variation of  $\gamma_o$  vs  $\gamma_r$  and, hence, on the transmissibility  $\gamma_o/\gamma_r$ . It is clear that reducing  $C_0$  reduces the transmissibility and thus the danger of local face contact. The differences between the analytical and numerical solutions for the transmissibility at rotor runouts,  $\gamma_r$ , corresponding to  $(h/C_0)_{min} = 0.25$  are between 1.4 and 12.4 percent depending on the design clearance. Here the largest percent error corresponds to the smallest design clearance. Figure 5(c) presents the effect of  $C_0$  on the axial displacement  $Z$ . The analytical solution assumes  $Z = 0$  at all times but from the numerical results it can be seen that, in reality, the rotor runout causes positive axial displacement; hence, the sealing gap opens up. This opening increases as  $\gamma_r$  increases. At  $\gamma_r$  values corresponding to  $(h/C_0)_{min} = 0.25$ , the axial displacements are 2.95  $\mu\text{m}$ , 1.96  $\mu\text{m}$ , and 0.88  $\mu\text{m}$  for clearances  $C_0$  of 12  $\mu\text{m}$ , 8  $\mu\text{m}$ , and 4  $\mu\text{m}$ , respectively. Hence, the smaller the design clearance, the smaller the axial displacement. It can be concluded, therefore, that a small design clearance is a preferable choice since it reduces the transmissibility, increases the minimum film thickness and reduces the axial displacement. Thus, it reduces both the danger of local face contact and the leakage across the seal.

Figure 5 presents the effect of shaft speed on the minimum film thickness, transmissibility, and axial displacement. From Fig. 5(a), we see that at a given runout,  $\gamma_r$ , a lower speed,  $\omega$ , results in a higher minimum film thickness,  $(h/C_0)_{min}$ . Lower speed also reduces the transmissibility [Fig. 5(b)] and the axial displacement [Fig. 5(c)].

Pressure differential effects are shown in Fig. 6. From Fig. 6(a), we see that for the two smaller pressure differential, namely, 0.1 MPa and 0.3 MPa, the analytical solutions for  $(h/C_0)_{min}$  are identical. This is also true for the numerical results at  $\gamma_r \leq 2$ . However, as  $\gamma_r$  increases the numerical results part and in the case of  $p_o - p_i = 0.1$  MPa, there seems even to be an increase in  $(h/C_0)_{min}$  for  $\gamma_r > 4$ . This is probably due to the sharp increase in the axial displacement  $Z$  [see Fig. 6(c)]. Although a large minimum film thickness prevents local face contact, one should also check whether this is not a result of large axial displacement which eventually causes seal failure because of high leakage. At

$(h/C_o)_{min} = 0.25$ , the analytical results for the corresponding  $\gamma$ , are from 20 to 30 percent smaller than the numerical results depending on the value of  $p_o - p_i$ . The better accuracy corresponds to the higher pressure. From Fig. 6(b),

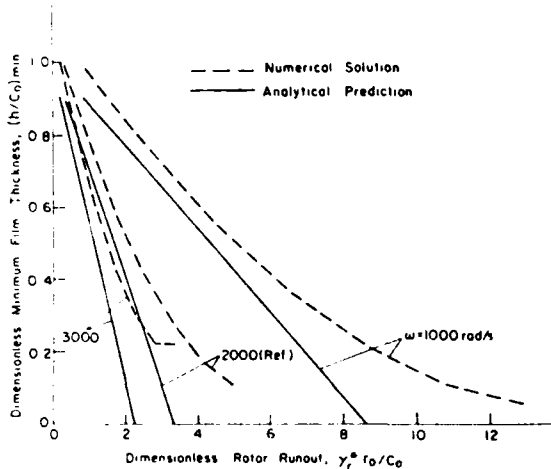


Fig. 5(a)—Minimum film thickness,  $(h/C_o)_{min}$ , vs rotor runout,  $\gamma_r$ , and shaft speed,  $\omega$ .

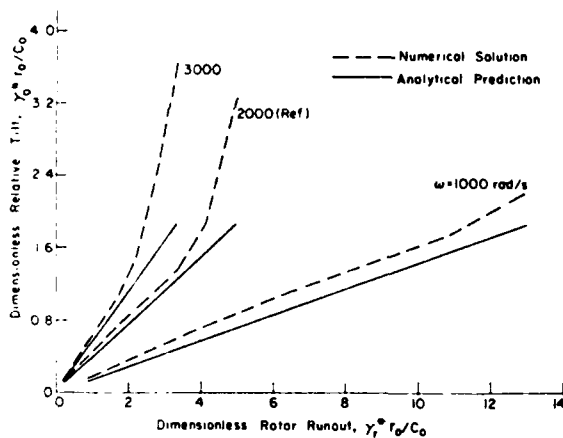


Fig. 5(b)—Relative tilt,  $\gamma$ , vs rotor runout,  $\gamma_r$ , and shaft speed,  $\omega$ .

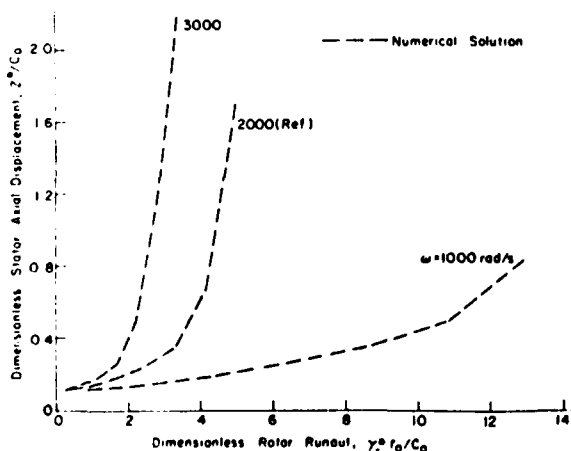


Fig. 5(c)—Axial displacement,  $Z$ , vs rotor runout,  $\gamma_r$ , and shaft speed,  $\omega$ .

it can be seen that increasing the pressure differential reduces the transmissibility, and hence, reduces the danger of local face contact. Figure 6(c) shows that higher pressure differential reduces the axial displacement  $Z$ . This is probably due to the suppression of cavitation effect which induces hydrodynamic axial force tending to open the sealing gap.

Figure 7 presents the effect of various flexible supports. Case I corresponds to a metal bellows, case II to a Buna N O-ring secondary seal, and case III to a Viton 75 O-ring secondary seal. From Fig. 7(a), it can be seen that the Buna N which provides the medium stiffness and damping is the best choice at the operating speed of the reference case. The Viton 75 gives the best correlation between the analytical and numerical results (about 18 percent at  $(h/C_o)_{min} = 0.25$ ). From Fig. 7(b), we see that the transmissibility  $\gamma_o/\gamma_r$  is almost unaffected by the variations in the flexible support. A similar conclusion can be drawn from Fig. 7(c) regarding the effect on the axial displacement.

Figure 8 presents the effect of face taper,  $H_r$ . The taper is related to the face coning by

$$H_r = \beta^*(r_o - r_i) \quad [18]$$

Hence, by Eqs. [18] and [17], the optimum face taper is

$$\left(\frac{H_r}{C_o}\right)_{opt} = \frac{2}{R_i} \quad [19]$$

and in our reference case for  $R_i = 0.8$  and  $C_o = 8 \mu\text{m}$  (see Table 1) the optimum taper is  $H_r = 20 \mu\text{m}$ .

From Fig. 8(a), we see that as the taper decreases the minimum film thickness increases; also, the correlation between the analytical and numerical solutions improves. Figure 8(b) shows that reducing the taper reduces the transmissibility, and Fig. 8(c) shows that the smallest axial displacement corresponds to the smallest taper. These results can be attributed to the increase in the fluid film damping,  $D_f$ , as the face coning decreases (6). From Fig. 8, it seems as if the smallest taper of  $10 \mu\text{m}$  is a better choice than the optimum coning which in our case is  $20 \mu\text{m}$ . This, however, is misleading because of the effect of the coning on the stability threshold and on the transition period before steady state is reached. As was stated before, small coning results in high fluid film damping and, hence, reduces the critical speed  $\omega_c$  (see Eq. [15]). For the reference case of Table 1, the ratio of critical speed to operating speed,  $\omega_c/\omega$ , is 2.5 for  $H_r = 40 \mu\text{m}$ , 2.51 for  $H_r = 20 \mu\text{m}$ , and 2.29 for  $H_r = 10 \mu\text{m}$ . Reducing the taper to  $H_r = 3 \mu\text{m}$ , for example, results in  $\omega_c/\omega = 1.26$  and the seal approaches its stability threshold. Further reduction of the taper would cause seal failure due to dynamic instability.

Another disadvantage of small taper, which in practical seals, is associated with high fluid film damping exceeding the critical value, is the slow decay of any disturbance of the dynamic system. In order to obtain the steady-state response shown in Fig. 8 at  $\gamma_r = 1.5$ , for example, 16 shaft revolutions were required for the case  $H_r = 10 \mu\text{m}$  compared to only 8 and 5 revolutions for the  $20 \mu\text{m}$  and  $40 \mu\text{m}$  tapers, respectively. Increasing the rotor runout to

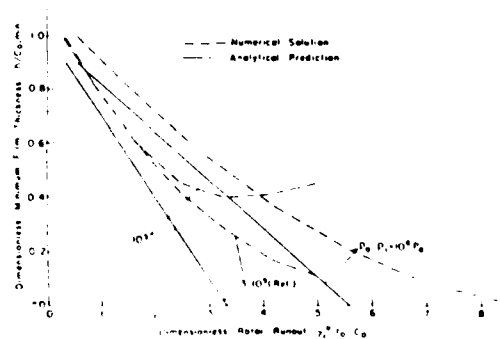


Fig. 6(a)—Minimum film thickness,  $(h/C_0)_{\min}$ , vs rotor runout,  $\gamma_r$ , and pressure differential,  $p_0 - p_i$ .

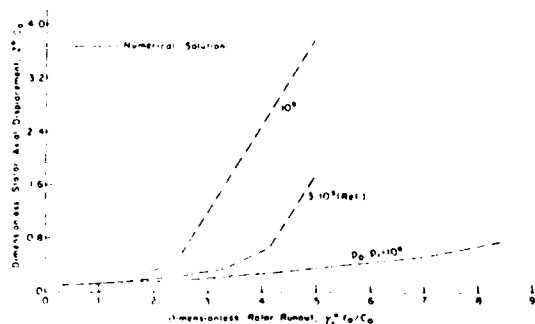


Fig. 6(b)—Relative tilt,  $\gamma$ , vs rotor runout,  $\gamma_r$ , and pressure differential,  $p_0 - p_i$ .

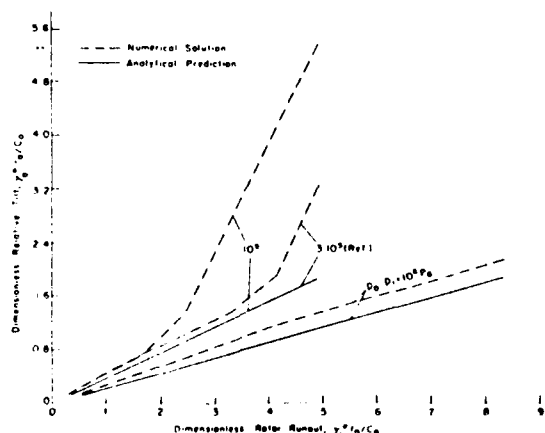


Fig. 6(c)—Axial displacement,  $Z$ , vs rotor runout,  $\gamma_r$ , and pressure differential,  $p_0 - p_i$ .

$\gamma_r = 5.6$ , for example, required 11 shaft revolutions to reach steady state at  $H_r = 20 \mu\text{m}$ , whereas at  $H_r = 10 \mu\text{m}$ , even 50 revolutions were not enough. Hence, it can be concluded that the optimum coning would be a better choice.

In general, Figs. 4 to 8 show that reducing the rotor runout  $\gamma_r$  increases the minimum film thickness and reduces both the transmissibility and the axial displacement. This results in a seal that operates with its faces closer to parallel

position and reduces the danger of failure due to local face contact or excessive leakage. As the rotor runout increases, the axial displacement increases, too. Since the leakage depends on  $C^3$ , and  $C = C_0(1 + Z)$ , an increase in  $Z$  has a very strong effect on the leakage. It seems that many seals may fail due to high leakage much before face rubbing as a result of critical rotor runout occurs.

Another important finding from Figs. 4 to 8 is the fact that the analytical prediction for the minimum film thickness  $(h/C_0)_{\min}$  is always below the numerical result and, hence, is on the safe side. This also means that the critical rotor runout found in (I) in the form

$$(\gamma_r)_{cr} = \frac{1}{T} - \gamma_d \quad [20]$$

(where  $T$  is the transmissibility  $\gamma_d/\gamma_r$ ) is a safe limit for design purposes.

In order to examine the effect of assembly tolerances on the dynamic behavior of the seal, an initial stator misalignment of  $\gamma_d = 3$  was selected. This misalignment corresponds to 0.6 mrad in the reference case of Table 1. With this misalignment added to the reference case, solutions were obtained at rotor runout values,  $\gamma_r$ , of: 0.3, 0.75, and 1.5 (corresponding to 0.06, 0.15, and 0.3 mrad, respectively). The analysis of Ref. (I) was used to calculate the stator response  $\gamma_d$  and it was found as  $\gamma_d = 0.129$  corresponding to 0.026 mrad in our reference seal. The critical rotor runout  $(\gamma_r)_{cr}$  in the presence of the stator initial misalignment was calculated [using (I)] and found to be 10 percent less than the critical value at  $\gamma_d = 0$ . Hence, initial stator misalignment reduces the critical rotor runout as can, indeed, be seen from Eq. [20].

Figures 9 through 11 present the steady-state response of the flexibly mounted stator in the presence of both rotor runout  $\gamma_r$  and initial stator misalignment,  $\gamma_d$ . In Fig. 9, the axial motion  $Z$  is shown, while Fig. 10 presents stator nutation  $\gamma_s$ , and Fig. 11 shows the variation in the phase angle  $\psi - \omega t$  (see Fig. 3) between the tilt vector of the stator  $\gamma_s$  and the tilt vector of the rotor,  $\gamma_r$ . The time base in these figures is expressed in shaft revolutions. From the three figures, it can be seen that the stator response consists of cyclic variations in  $Z$ ,  $\gamma_s$ , and the phase angle, and that the frequency of these variations is equal to the frequency of the shaft rotation. Such behavior was already predicted in (I) and also observed experimentally (7), (8). It should be noted here that while the small perturbation analysis (I) can predict the variations in  $\gamma$  and the phase angle between  $\gamma_s$  and  $\gamma_r$ , the time variation in  $Z$ , which is due to the coupling between the axial and angular degrees of freedom, can be predicted only by the numerical solution which takes account of the nonlinear effects.

From Fig. 9, we see that the amplitude of the axial motion increases with an increase of the rotor runout. In all three runout cases, the axial motion takes place about an average value of  $Z$  which is always positive. Hence, the average sealing gap is always larger than the design clearance  $C_0$ .

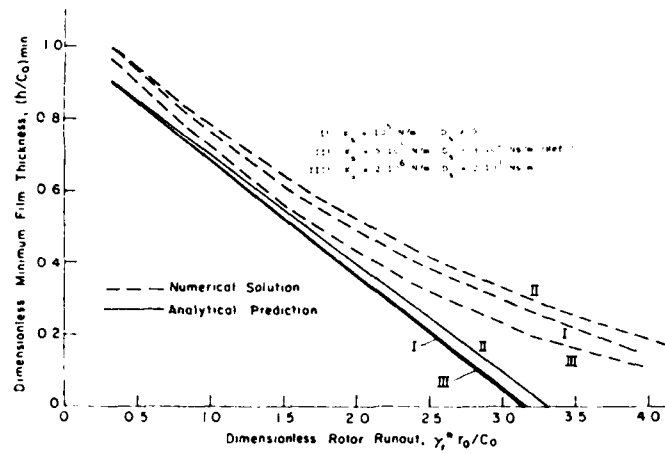


Fig. 7(a)—Minimum film thickness,  $(h/C_0)_{min}$ , vs rotor runout,  $\gamma_r$ , for various types of elastic support.

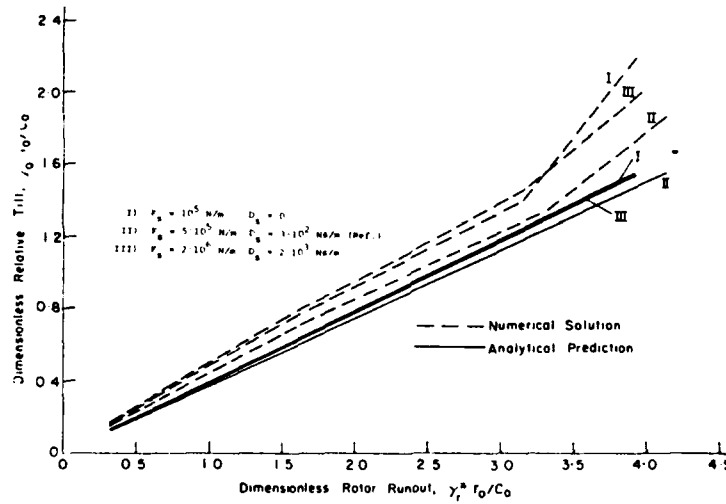


Fig. 7(b)—Relative tilt,  $\gamma$ , vs rotor runout,  $\gamma_r$ , for various types of elastic support.

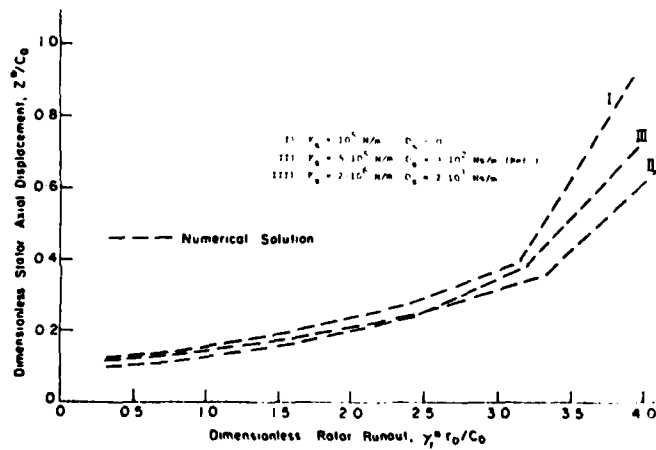


Fig. 7(c)—Axial displacement,  $Z$ , vs rotor runout,  $\gamma_r$ , for various types of elastic support.

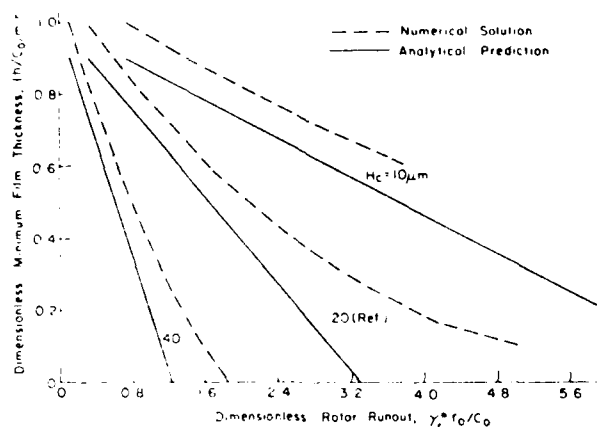


Fig. 8(a)—Minimum film thickness,  $(h Co)_{min}$ , vs rotor runout,  $\gamma_r$ , and cone height,  $H_c$ .

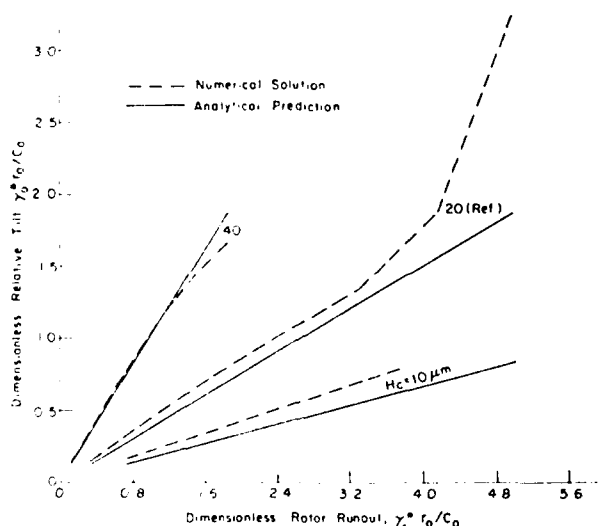


Fig. 8(b)—Relative tilt,  $\gamma$ , vs rotor runout,  $\gamma_r$ , and cone height,  $H_c$ .

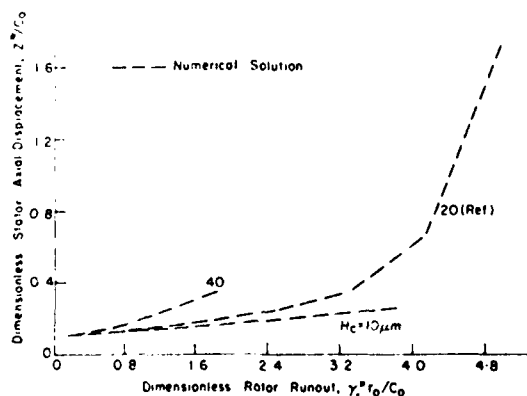


Fig. 8(c)—Axial displacement,  $Z$ , vs rotor runout,  $\gamma_r$ , and cone height,  $H_c$ .

From Fig. 10, it can be seen that the amplitude of  $\gamma$  is almost independent of the runout  $\gamma_r$ , while the average value of  $\gamma$  is strongly affected by  $\gamma_r$ . Referring to Fig. 3, we can assume that, similar to the small perturbation analysis (1),

the vector  $\vec{\gamma}$  can be combined of a fixed vector  $\vec{\gamma}_d$  which depends on  $\gamma_r$  alone, and a rotating vector  $\vec{\gamma}_s$ , which depends on  $\gamma_r$  alone. In this case, the maximum value of  $\gamma$  is the sum  $\gamma_r + \gamma_d$  and the minimum value of  $\gamma$  is  $\gamma_r - \gamma_d$ . This yields an average value that is equal to  $\gamma_r$ , and an amplitude that is equal to  $\gamma_d$ . The amplitudes of  $\gamma$ , in Fig. 10 corresponding to  $\gamma_r$  0.3, 0.75 and 1.5 are: 0.166, 0.166, and 0.163, respectively. The analytical value of  $\gamma_d$  found by using (1) is  $\gamma_d = 0.129$  which is about 20 percent less than the numerical amplitude. The average values of  $\gamma$ , in Fig. 10 corresponding to  $\gamma_r$  0.3, 0.75, and 1.5 are: 0.312, 0.774, and 1.540, respectively. The analytical values of  $\gamma_r$ , calculated by the small perturbation analysis for the three  $\gamma_r$  values are: 0.321, 0.803, and 1.606, respectively. Hence, the analytical  $\gamma_r$  values are only about 4 percent higher than the numerical average values of  $\gamma_r$ .

We can conclude, therefore, that Eq. [1] is valid in both the linear and nonlinear analyses and that there is a good correlation between the two cases.

The phase angle between the vectors  $\vec{\gamma}_r$  and  $\vec{\gamma}$ , (see Fig. 3) is shown in Fig. 11 as a function of time. For the large runout values ( $\gamma_r = 0.75$  and  $\gamma_r = 1.5$ ) the phase angle is negative throughout the period, that is, the stator tilt vector,  $\vec{\gamma}_s$ , always lags the rotor tilt vector,  $\vec{\gamma}_r$ . For the small runout,  $\gamma_r = 0.3$ , the phase angle is negative over most of the period but here, alternately, the tilt of the rotor and that of the stator is in the lead. This behavior was observed experimentally and reported in (8).

## CONCLUSION

A computer program was used to solve the complete set of the nonlinear equations of motion of the flexibly mounted stator in a noncontacting coned-face mechanical seal. Rotor runout as well as assembly tolerances in the form of initial stator misalignment were accounted for. Cavitation in the fluid film between the mating faces was also taken into account. The computer program enables transient analysis of the seal dynamics and provides simulation of the seal behavior. Both stability threshold and steady-state response of the flexibly mounted stator were investigated.

In general, it was found that the critical shaft speed corresponding to stability threshold is quite high. Hence, the dynamic stability should not be a problem in the majority of noncontacting seals. A more practical problem in noncontacting seals is the steady-state dynamic response of the stator resulting from rotor runout and assembly tolerances. The stator steady-state response is a nonsynchronous tracking of the rotor runout with cyclic variations in the seal clearance, the relative misalignment between its mating faces, and in the phase angle between stator and rotor tilts. A parametric investigation was performed to explore the effect of various design parameters and operation conditions on the seal behavior. A critical runout was found that, if exceeded, results in seal failure due to local face contact. It was also found that seals may fail because of an excessive leakage resulting from an increase in the seal clearance much before the critical runout is reached. This can happen in seals with low stiffness of the fluid film and the flexible support. Small design clearance, high pressure differential,

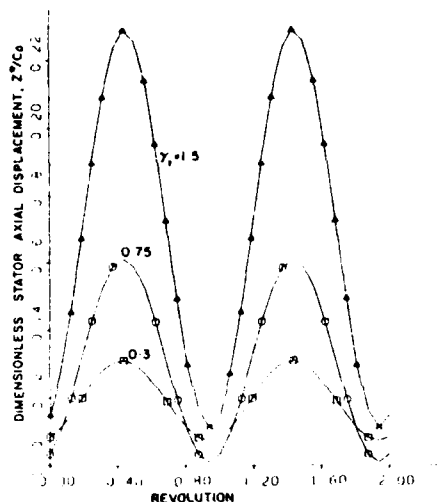


Fig. 9—Time variation of the axial displacement,  $Z$ , at an initial stator misalignment,  $\gamma_w = 3$ , and various rotor runouts,  $\gamma_r$ .

and optimum coning provide high stiffness of the fluid film and reduce the danger of a too high operating clearance.

The results of the numerical analysis were compared with the results of a small perturbation analysis that provides much simpler closed form analytical solution. Very good correlation was found between the two analyses for most cases of practical applications. Fair correlation was found even in cases which are clearly out of the range of small perturbation. In these cases, the small perturbation analysis yields results that are on the safe side with regard to the critical rotor runout. If a practical limit is set for the permissible minimum film thickness at, say, 25 percent of the design clearance, then the analytical results of the small perturbation analysis can probably be valid over the full range of design parameters and operation conditions.

#### ACKNOWLEDGMENT

The research reported here was supported in parts by the Israel Academy of Sciences and the US Air Force Wright Aeronautical Labs/AFWAL/POSL under contract F49620-83-C-0057.

#### REFERENCES

- (1) Green, I. and Etsion, I., "Stability Threshold and Steady State Response of Noncontacting Coned Face Seals," ASLE Preprint No. 84-IC-5A-2, Oct. 1984.
- (2) Green, I. and Etsion, I., "Stiffness and Damping Characteristics of Elastomer O-rings Secondary Seals Subjected to Reciprocating Twist," *Proc. 10th Intl. Conf. on Fluid Sealing*, BHRA, pp 221-229, April (1984).
- (3) Etsion, I., "Dynamic Analysis of Noncontacting Face Seals," *Trans. ASME J. Lub. Tech.*, **104**, 1, pp 460-468 (1982).

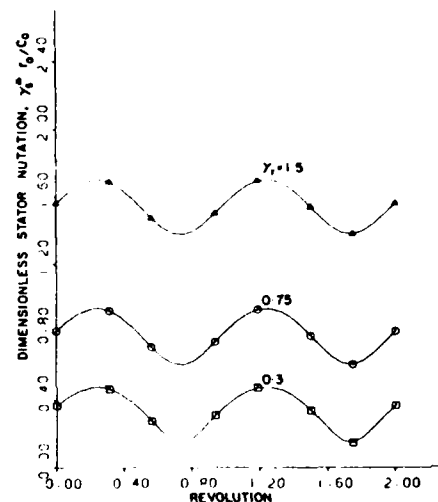


Fig. 10—Time variation of the nutation,  $\gamma_n$ , at an initial stator misalignment,  $\gamma_w = 3$ , and various rotor runouts,  $\gamma_r$ .

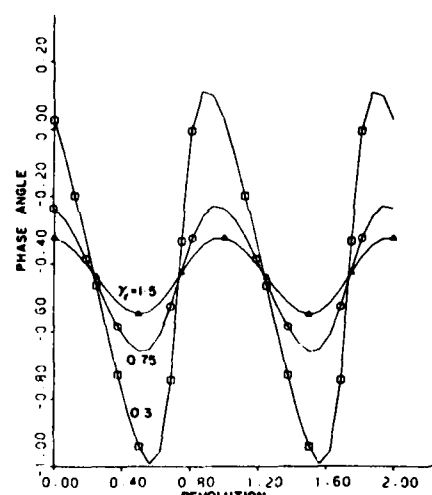


Fig. 11—Time variation of the phase angle at an initial stator misalignment,  $\gamma_w = 3$ , and various rotor runouts,  $\gamma_r$ .

- (4) Auer, B. M. and Etsion, I., "Computer Program Documentation For the Dynamic Analysis of a Noncontacting Mechanical Face Seal," NASA TM-81636, Nov. 1980.
- (5) Speckhart, H. F. and Green, I. W., *A Guide to Using CSMP—The Continuous System Modeling Program*, Prentice-Hall Inc., New Jersey (1976).
- (6) Green, I. and Etsion, I., "Fluid Film Dynamic Coefficients in Mechanical Face Seals," *Trans. ASME J. Lub. Tech.*, **105**, 2, pp 297-302 (1983).
- (7) Sehnal, J., Sedý, J., Zohens, A., and Etsion, I., "Performance of the Coned-Face End Seal with Regard to Energy Conservation," *ASLE Trans.*, **26**, 4, pp 415-429 (1983).
- (8) Etsion, I. and Constantinescu, I., "Experimental Observation of the Dynamic Behavior of Noncontacting Coned-Face Mechanical Seals," *ASLE Trans.*, **27**, 3, pp 263-270 (1984).

Presented at the 40th ASLE Annual Meeting in Las Vegas, Nevada, May 6-9, 1985. This paper is the literary property of the American Society of Lubrication Engineers. The Press may summarize freely from this manuscript after presentation, citing source; however, publication of material constituting more than 20 percent of the manuscript shall be construed as a violation of the Society's rights and subject to appropriate legal action. Manuscripts not to be published by the Society will be released in writing for publication by other sources. Statements and opinions advanced in papers are understood to be individual expressions of the author(s) and not those of the American Society of Lubrication Engineers.

**END**

**FILMED**



**DTIC**